Applied Energy 406 (2026) 127316

Contents lists available at ScienceDirect

Applied Energy

journal homepage: www.elsevier.com/locate/apenergy

Innovations and prospects on functional membrane design for advanced redox flow batteries

Jiaojiao Deng [a], Dongqing Pang [a], Xiaoliang Yu [b], Yu Bai [b], Jinhan Mo [a,c,d,*]

[a] Key Laboratory of Coastal Urban Resilient Infrastructures (Ministry of Education), College of Civil and Transportation Engineering, Shenzhen University, Shenzhen, Guangdong 518060, China
[b] Department of Mechanical Engineering and Research Institute for Smart Energy, The Hong Kong Polytechnic University, Hong Kong 999077, China
[c] State Key Laboratory of Subtropical Building and Urban Science, Shenzhen University, Shenzhen 518060, China
[d] State Key Laboratory of Intelligent Geotechnics and Tunnelling, Shenzhen University, Shenzhen 518060, China

HIGHLIGHTS

- Advanced membrane design for redox flow batteries is comprehensively reviewed.
- Fundamental ion transport mechanisms and performance trade-offs are elucidated.
- Innovative dense, porous, and charged microporous membrane architectures are outlined.
- Future studies focus on advanced modeling, normalized test, and system optimization.

GRAPHICAL ABSTRACT

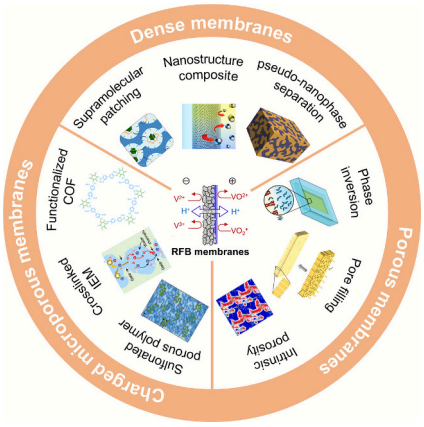

ARTICLE INFO

Keywords:
Redox flow battery
Membrane
Conductivity
Selectivity
Stability
Microstructure

ABSTRACT

Conventional membrane design for redox flow batteries (RFBs) faces persistent challenges in balancing the conductivity–selectivity–stability trilemma, particularly with perfluorinated benchmark materials suffering from high cost, redox couple crossover, and environmental concerns. Recent advances demonstrate that microstructure engineering and novel chemistries, including charged/uncharged nanochannels, size-exclusion architectures, and hybrid systems, enable breakthrough performance. However, comprehensive reviews linking these innovations to commercialization barriers remain limited. This review presents a novel synthesis of recent advances in RFB membrane design by structurally categorizing membranes into dense, porous, and charged microporous types, and highlights innovative strategies that overcome the classic conductivity–selectivity–stability trade-off. We first establish the fundamental ion transport mechanisms and performance trade-offs governing membrane efficiency; multifunctional chemistries and microstructural control of RFB membranes are also

* Corresponding author at: Key Laboratory of Coastal Urban Resilient Infrastructures (Ministry of Education), College of Civil and Transportation Engineering, Shenzhen University, Shenzhen, Guangdong 518060, China.
E-mail address: mojinhan@szu.edu.cn (J. Mo).

https://doi.org/10.1016/j.apenergy.2025.127316
Received 25 August 2025; Received in revised form 27 November 2025; Accepted 22 December 2025

analyzed. Subsequently, we categorize membrane architectures into dense and porous configurations based on structural features, and highlight recent innovations that overcome conductivity-selectivity compromises through Donnan exclusion in charged dense membranes, size sieving in porous membranes, and the synergy between the two in charged porous membranes. Finally, we discuss unresolved challenges in long-term stability, scalability, performance validation, and integrated system design, providing a roadmap for future research focused on operando characterization, bio-inspired multifunctional materials, and system-specific optimization. This review establishes design principles for next-generation RFB membranes that simultaneously achieve high efficiency, durability, and eco-compatibility in grid-scale energy storage.

1. Introduction

The global transition to renewable energy requires advanced grid-scale storage solutions to address the intermittency of sources such as solar and wind and to ensure grid stability [1,2]. Among various energy storage technologies [3–7], redox flow batteries (RFBs), particularly vanadium-based redox flow batteries (VRFBs), have emerged as promising candidates due to their ability to decouple power and energy ratings, inherent safety derived from aqueous electrolytes, and scalability [8,9]. As a critical component of RFBs, the membrane must simultaneously fulfill three competing requirements: i) high ion selectivity to block crossover of redox-active species while facilitating charge-balancing ion transport; ii) low ionic resistance to minimize energy losses and maximize voltage efficiency; and iii) robust chemical and mechanical stability to withstand harsh electrochemical environments over long operational lifetimes. These demands give rise to a fundamental conductivity−selectivity−stability trilemma, These demands give rise to a fundamental conductivity–selectivity–stability trilemma, which constitutes a major constraint on the widespread deployment of RFB technology [10–12].

Commercial perfluorosulfonic acid (PFSA) membranes exemplify this fundamental trade-off. They exhibit exceptional proton conductivity, often exceeding 90 mS cm^{-1}, and demonstrate remarkable chemical and mechanical durability under operating conditions. However, these advantages are offset by several critical drawbacks: high vanadium ion permeability (6.72×10^{-6} cm^2 min^{-1}), which leads to significant capacity fade and efficiency loss; prohibitively high cost, contributing to over 40 % of the total stack expense; and the environmental persistence of perfluoroalkyl substances, raising concerns over ecological impact and long-term sustainability [13,14]. Hydrocarbon-based membranes represent cost-effective alternatives to PFSAs; however, their practical application is limited by susceptibility to oxidative degradation, primarily through cleavage of C—H bonds [15,16]. Moreover, inherent material trade-offs further limit performance. For example, enhancing conductivity typically necessitates the incorporation of hydrophilic domains, which increases water uptake and causes swelling. This process expands the membrane's transport pathways and accelerates vanadium ion crossover. [17]. Similarly, reducing membrane thickness lowers area-specific resistance but compromises mechanical strength and further promotes crossover [18]. These limitations greatly hinder the commercial viability of hydrocarbon membranes for long-duration flow battery applications.

Recent advances in membrane design emphasize precise microstructural control and novel chemical approaches to address existing challenges. In dense membranes, rigid sub-nanometer channels (less than 2 nm) utilize nanoconfinement effects to improve size-selective sieving and strengthen ion–pore interactions. This process facilitates ultra-selective ion transport, frequently via continuous hydrogen-bonding networks or Grotthuss-type proton conduction pathways [19]. Moreover, porous membranes are created using techniques such as phase inversion or sacrificial templating. These membranes are engineered with well-defined nanopores (ranging from 1 to 5 nm) that facilitate efficient size-exclusion sieving while keeping area-specific resistance low [20,21]. Hybrid systems also play a crucial role by incorporating functional nanofillers into polymer matrices, which helps to tailor ionic pathways and improve selectivity in composite membranes [22–24]. Additionally, layered architectures combine mechanically robust porous supports with thin selective layers, effectively decoupling the traditional trade-off between conductivity and selectivity [25,26].

Despite these advances, comprehensive reviews linking these innovations to commercialization barriers are still limited [10,27]. This review presents a novel synthesis of recent advances in RFB membrane design by structurally categorizing membranes into dense, porous, and charged microporous types, and highlights innovative strategies that overcome the classic conductivity–selectivity–stability trilemma. Fundamental ion transport mechanisms and performance trade-offs in membranes are first established, and multifunctional chemistries and microstructural control are also critically analyzed. Then, membrane architectures are classified into dense and porous types according to their structural characteristics, with emphasis on recent advances that address conductivity–selectivity trade-offs via Donnan exclusion in charged dense membranes, size-sieving in porous membranes, and synergistic strategies in charged porous systems. Persisting challenges in long-term stability, scalability, and performance validation are examined, concluding with a research roadmap emphasizing operando characterization, bio-inspired multifunctional materials, and system-specific optimization. This review, while centered on VRFB membranes for illustrative depth, will highlight membrane strategies that are applicable or have been successfully demonstrated across these and other emerging RFB systems, such as aqueous organic RFBs [28–32] and iron-chromium RFBs [33–36]. By integrating chemistry, microstructure, and sustainability perspectives, this work bridges lab-scale innovations with industrial deployment needs, ultimately enabling membranes that simultaneously achieve low resistance, high selectivity, and long lifespan for grid-scale renewable energy storage.

2. Fundamentals of RFB membranes

RFBs store energy in electrolyte solutions containing dissolved redox-active species, such as vanadium ions and organic molecules. During battery operation, these electrolytes are pumped from external tanks through electrochemical cells where oxidation and reduction reactions take place at the porous surface of electrodes (Fig. 1). The membrane serves as a critical component by performing two essential functions: it physically separates the catholyte and anolyte to prevent cross-mixing of active species, while selectively facilitating the transport of charge-balancing ions to maintain electroneutrality throughout charge and discharge cycles. In conventional vanadium RFBs (VRFBs), the reactions at two electrodes are as shown in Eqs. 1 and 2 [10].

$$\textit{Positive electrode}: VO^{2+} + H_2O \underset{\text{Discharge}}{\overset{\text{Charge}}{\rightleftarrows}} VO_2{}^{+} + 2H^{+} + e^{-} \quad (1)$$

$$\textit{Negative electrode}: V^{3+} + e^{-} \underset{\text{Discharge}}{\overset{\text{Charge}}{\rightleftarrows}} V^{2+} \quad (2)$$

Selective ion transport through membranes plays a key role in the RFB operation [37]. Therefore, in this section, we will first summarize the ion transport mechanisms in RFB membranes. Subsequently, various performance metrics of RFB membranes will be discussed, focusing

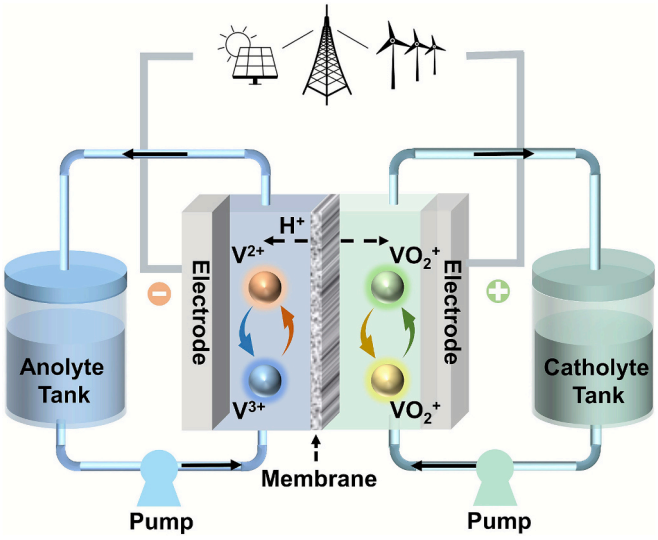

Fig. 1. Schematic diagram of the working principle of vanadium-based RFBs.

primarily on conductivity, selectivity, and stability. Next, membrane composition, which is the intrinsic factor influencing these performance metrics, is summarized, with a brief overview of the relationship between composition and electrochemical properties. Finally, primary structural configurations of current RFB membranes, such as dense membranes, porous membranes, and charged microporous membranes, are outlined.

2.1. Ion transport mechanisms in RFB membranes

Membranes in RFBs enable critical functions in electrochemical systems by facilitating selective ion transport while separating electrode reactions. Their performance hinges on ion transport dynamics within charged channels, governed by complex interactions between ions, functional groups, and the membrane matrix. Traditional ion-exchange membranes rely on microphase-separated nanostructures (typically >2 nm) formed by hydrophilic/hydrophobic domain segregation [38]. In these systems, ion transport follows the Donnan-Manning model, where counter-ion mobility depends on nanochannel tortuosity described by the Mackie-Meares model and electrostatic effects modeled by Manning's counter-ion condensation theory [39]. While effective for basic cation/anion separation, these membranes face an intrinsic permeability/selectivity trade-off: increasing ion exchange capacity to enhance conductivity inevitably causes water uptake-induced swelling, enlarging channels, and compromising selectivity among similarly charged ions.

The emergence of new-generation membranes with rigid microporous channels (< 2 nm) fundamentally changes the ion transport behavior. These membranes leverage confinement effects at sub-nanometer scales to intensify size sieving and ion-channel interactions. Key breakthroughs arise from three classifications of channel dimensions. Sub-2-nm channels (1–2 nm) enable hydrated ion transport while amplifying interactions with functionalized pore walls [40]. Sub-1-nm channels (0.7–1 nm) force partial dehydration of ions, weakening hydration shell shielding and significantly enhancing electrostatic interactions [41]. Ultramicropores (< 0.7 nm) induce near-complete dehydration, which exposes intrinsic ion properties and enables ultra-selective transport through continuous hydrogen-bond networks or Grotthuss mechanisms.

Ion flux (J_i) in charged channels follows the Nernst-Planck equation, coupled with the Poisson equation [42,43] to account for electric field-concentration gradient, as presented in Eqs. 3 and 4 [44].

$$J_i = -D_i\nabla c_i - \frac{z_i F}{RT} D_i c_i \nabla\Phi \tag{3}$$

$$\nabla^2\Phi = -\frac{e}{\varepsilon}(c_+ - c_-) \tag{4}$$

where J_i, D_i, c_i, c_+, c_-, z_i, and Φ are the ion flux, diffusion coefficient, ion concentration, cation concentration, anion concentration, ionic species' valence, and chemical potential, respectively.∇ denotes the gradient operator, and ∇^2 is the Laplace operator. F, R, T, e, and ε are the Faraday constant, universal gas constant, Kelvin temperature, electron charge, and dielectric constant, respectively.

The behavior of ion transport is dictated by the channel diameter (d) relative to the Debye length (λ_D) [45]. When $d > 2\lambda_D$, bulk-like ion transport dominates with negligible selectivity. As the channel size decreases ($d < 2\lambda_D$), overlap of the electrical double layers occurs, promoting counter-ion accumulation and enhancing selectivity. Further confinement, where λ_D is less than 1 nm and d approaches hydrated ion diameters, leads to dominance by confinement effects: partial dehydration lowers the energy barrier for specific ions via tailored interactions, such as electrostatic forces, hydrogen bonding, and coordination.

2.2. Key performance parameters of RFB membranes

The performance of RFBs rely critically on the membrane's key parameters. High ionic conductivity minimizes energy loss by facilitating efficient ion transport, and exceptional selectivity is vital to allow desired ions to pass while blocking active species crossover, preventing self-discharge and capacity fade. Simultaneously, the membrane must possess robust mechanical stability to withstand operational stresses such as pressure gradient without tearing, and outstanding chemical stability to resist degradation from harsh electrolyte corrosion over thousands of cycles. Optimizing these properties, including conductivity, selectivity, mechanical strength, and chemical resilience, is essential for achieving efficient, durable, and cost-effective RFB operation [46]. Noteworthy that membrane requirements in RFBs are system-specific, dictated by the redox couples. VRFBs demand blocking multivalent vanadium cations in acidic, oxidizing environments [27]. Aqueous organic RFBs require precise size-exclusion to hinder organic molecule crossover across varying pH levels [47]. Iron-chromium RFBs need selective Fe/Cr separation and stability in corrosive chloride electrolytes [48]. Thus, while the conductivity-selectivity-stability trilemma is universal, optimal membrane design is chemistry-dependent.

2.2.1. Conductivity

Conductivity (σ, S cm^{-1}) dictates voltage efficiency and power density. Ion conduction is based on the vehicle mechanism and the Grotthuss mechanism [49]. The former involves hydrated ion diffusion through hydrophilic domains. And the latter is derived from ion hopping between protonation sites, such as $-SO_3H$ groups and N-heterocycles.

Ion transport in RFB membranes is governed by three interconnected factors. Water uptake and hydrophilicity establish the foundation for ion mobility by enabling solvation and hydration of charge carriers. Ion-exchange capacity, particularly the density of functional groups like $–SO_3^-$, directly enhances conductivity but simultaneously exacerbates membrane swelling. Critically, the microstructure exemplified by well-connected hydrophilic channels in phase-separated materials such as PFSA determines the efficiency of ion conduction pathways. These factors exhibit an inherent trade-off: strategies that boost conductivity often exacerbate swelling, which widens transport pathways and accelerates detrimental vanadium crossover [50]. This compromise remains a central challenge in membrane design. Additionally, temperature significantly influences ion conductivity [16,51]. Elevated temperatures typically enhance ion mobility and reduce electrolyte viscosity, thereby increasing conductivity and improving voltage

efficiency [52]. However, this benefit must be balanced against accelerated membrane degradation and increased crossover rates at higher temperatures [53].

2.2.2. Selectivity & permeability

Selectivity can be determined by the ratio of conductivity to permeability (σ/P). It evaluates the membrane's ability to balance high ion conduction with low active-species crossover. And permeability quantifies undesired ion crossover. **Three synergistic strategies can be used to enhance membrane selectivity in RFBs.** Size exclusion utilizes precisely engineered nanopores in materials like polymers of intrinsic microporosity (PIMs) or porous membranes to physically block larger hydrated redox species while permitting smaller charge-balancing ions to permeate [54]. Complementarily, Donnan exclusion leverages fixed charged groups to electrostatically repel similarly charged active species [55]. For instance, anion-exchange membranes with $-NR_3^+$ groups effectively repel cationic vanadium ions. To overcome inherent limitations of single-mechanism designs, hybrid approaches integrate thin selective layers onto porous supports, combining size-sieving precision with Donnan repulsion to achieve hierarchical selectivity without compromising conductivity [25].Besides, operational temperature critically influences membrane performance. Elevated temperatures typically increase water uptake, promoting higher ionic conductivity but also inducing greater swelling [56]. This swelling can compromise mechanical stability and accelerate species crossover, creating a key trade-off for membrane design and operational control. Therefore, temperature is a vital parameter in assessing membrane suitability for practical RFB applications.

2.2.3. Stability

The operational lifespan of RFBs necessitates that membranes endure harsh electrochemical environments, including exposure to strong acids or bases, potent oxidizing agents, and sustained mechanical stress, for extended periods exceeding 10 to 20 years [57]. Mechanical stability is a primary requirement, demanding robust tensile strength to resist physical stresses encountered during cell assembly, stack compression, and operational pressure fluctuations, thereby preventing catastrophic membrane rupture. Concurrently, dimensional stability, characterized by a low swelling ratio upon electrolyte uptake, is equally critical. Minimizing swelling is essential to preserve the integrity of selective transport pathways, as it reduces pore distortion and effectively curtails the undesired permeation of active species, such as vanadium ions. To simultaneously achieve high mechanical robustness and controlled swelling, current research employs strategies such as chemical crosslinking to fortify the polymer network, blending with dimensionally stable components, and implementing reinforcement via layered architectures. These approaches collectively ensure structural integrity while suppressing performance-degrading swelling [58].

Chemical stability is paramount for RFB membranes operating in harsh electrochemical environments, particularly in vanadium systems where highly oxidative VO_2^+ species necessitate robust oxidation resistance. Membrane degradation under extreme pH conditions proceeds through distinct mechanisms: hydrocarbon-based polymers are susceptible to oxidative cleavage of C—H and C—C bonds, while anion-exchange membranes face nucleophilic attacks targeting vulnerable functional groups, such as quaternary ammonium moieties. To mitigate these failure pathways and enhance longevity, recent research has focused on several material strategies. These include utilizing inherently stable fluorinated backbones [59], oxidation-resistant aromatic polymers [20], and protective additives such as radical scavengers that quench reactive species before membrane damage occurs [60].

It is important to note that temperature acts as a critical accelerator for these degradation mechanisms [30]. Higher operational temperatures can dramatically increase the rate of oxidative attacks, hydrolysis of functional groups, and polymer chain scission, thereby shortening the membrane's lifespan. Consequently, the evaluation of membrane stability must account for temperature-dependent degradation, and long-term durability tests should be conducted under relevant thermal conditions to accurately predict performance over the battery's operational lifetime.

Furthermore, operational temperature emerges as a pivotal external parameter that critically influences this balance. It directly modulates ion transport, swelling behavior, and chemical degradation rates, thereby making the optimization of membrane properties inherently temperature-specific. A comprehensive understanding of these thermal effects is indispensable for developing membranes capable of delivering stable performance under real-world operating conditions.

Table 1 summarizes the impact of various parameters on RFB performances, their key influencing factors, and optimization strategies. Achieving simultaneous optimization of conductivity, selectivity, and stability in RFB membranes remains fundamentally challenging due to inherent material trade-offs. Enhanced ion conductivity requires hydrophilic domains that facilitate ion solvation and mobility, yet membrane swelling in these regions enlarges transport pathways, accelerating vanadium crossover and degrading selectivity. Stability–cost conflicts arise with benchmark PFSA membranes like Nafion. On the one hand, they offer exceptional chemical/mechanical robustness; on the other hand, their high cost and environmental footprint limit scalability [61]. In stark contrast, hydrocarbon alternatives reduce costs but sacrifice long-term stability under harsh operating conditions [62]. Thinning membranes reduce ionic resistance but exacerbate fragility and crossover susceptibility, forcing compromises between performance efficiency and durability.

2.3. Composition of RFB membranes

RFB membranes primarily comprise three material categories: PFSA-based polymers, functionalized aromatic hydrocarbon polymers, and heterocyclic polybenzimidazole (PBI), as summarized in Table 2. PFSA membranes, exemplified by commercial Nafion, dominate current applications due to their exceptional proton conductivity (>100 mS cm^{-1}) and robust mechanical/chemical stability in acidic environments. However, their inherent limitations, including high vanadium ion crossover from oversized hydrated channels, substantial material cost, and environmental persistence, drive research toward non-fluorinated alternatives [63].

Functionalized aromatic hydrocarbon polymers are promising candidates [64]. Aromatic polymers, including sulfonated poly(ether ether ketone) (SPEEK) [57,65,66], sulfonated polysulfone (SPSF) [67], sulfonated poly(ether sulfone) (SPES) [61], and chloromethylated/

Table 1
Summary of various parameters' impact on RFB performances, their key influencing factors, and optimization strategies.

Parameter	Impact on RFB	Key Influencing Factors	Optimization Strategies
Conductivity	Voltage efficiency, power density	Water uptake, hydrophilicity, microstructure, temperature	Hydrophilic grafts, acid-doping, phase-separated designs
Selectivity	CE, capacity retention	Pore size, charge density, Donnan potential, temperature	Size exclusion, charged grafts, LbL coatings
Permeability	Self-discharge, capacity fade	Swelling ratio, ion size, membrane charge, temperature	Crosslinking, nanofillers, hydrophobic segments
Mechanical Stability	Cycle life, durability	Tensile strength, swelling ratio, crosslink density, temperature	Reinforcing layers, polymer blending, crosslinking
Chemical Stability	Long-term operation	Backbone chemistry, oxidation resistance, hydrolytic stability, temperature	Fluorination, stable aromatics, antioxidant additives

Table 2
Molecular structure summary of various polymer membranes for RFBs.

Polymer		Molecular structure	Ref.
PFSA		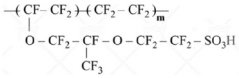	[85]
PBI	Original PBI	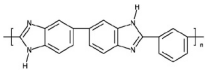	[86]
	Acid-doped PBI	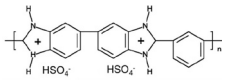	[86]
	MS-PBI	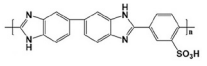	[87]
	PBI-OSO_3−/OHN+	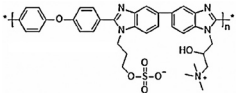	[88]
PEEK	Original PEEK	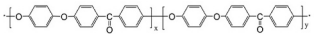	[89]
	SPEEK	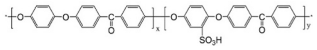	[89]
	BSEEK	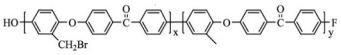	[90]
PSF	Original PSF	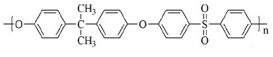	[91]
	SPSF	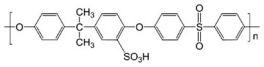	[92]
	CMPSF	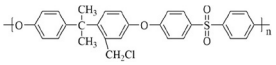	[91]
PES	Original PES	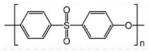	[93]
	SPES	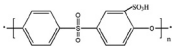	[94]
SPI	Original SPI	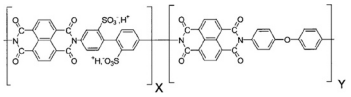	[95]
	Branched SPI	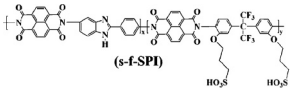	[96]

quaternized derivatives (CMPSF/QAPSF) [68] offer cost-effective, tunable platforms. These materials require deliberate functionalization, such as sulfonation and quaternization, to introduce ion-exchange groups such as $-SO_3^-$ and $-NR_3^+$ that enable proton transport. Unmodified versions exhibit negligible conductivity, but post-modification conductivity remains lower than PFSA. Critically, excessive functionalization degrades chemical stability in oxidizing electrolytes like VO_2^+ solutions and exacerbates swelling, leading to mechanical fragility and vanadium permeation [69]. Molecular design variations, such as branched sulfonated polyimide (SPI) architectures, enhance entanglement density, reducing vanadium diffusion and partially mitigating stability issues.

PBI represents a distinct class of heterocyclic aromatic membranes with exceptional oxidative stability [57,70,71]. Its proton conductivity relies on acid doping rather than intrinsic ion-exchange groups [72]. Immersion in sulfuric acid facilitates dual proton-transport pathways: 1) protonation of imidazole nitrogen sites and 2) retention of free acid within the polymer matrix. Conductivity correlates with acid doping levels and membrane hydration [73]. Notably, molecular flexibility and imidazole group density critically influence performance. For instance, polymers like poly[4,4′-(diphenylether) − 5,5′-bibenzimidazole] (OPBI) [74], with flexible chains and low imidazole density, achieve higher conductivity than rigid, highly functionalized analogues, such as poly (2,5-benzimidazole) (ABPBI), by minimizing hydrogen-bond network resistance [75]. Sulfonation of PBI further boosts conductivity but risks compromising stability [76].

Other polymers, such as phosphinated polypentafluorostyrene [77], polyvinylidene fluoride (PVDF) [78], polytetrafluoroethylene (PTFE) [79], and polypropylene [80], have been explored for niche advantages. Modifications like polymer blending, nanofiller integration, and cross-linking aim to balance conductivity−selectivity trade-offs [81,82]. For instance, PFSA modification via zwitterionic grafting leverages charge repulsion to curb vanadium crossover [83]. Similarly, cross-linking with bipyridine networks achieves high ion selectivity through Donnan exclusion [84].

2.4. Microstructures of RFB membranes

Membranes in RFBs can be categorized into dense and porous ones. The core operational difference between these two lies intrinsically in their microstructures and the consequent primary mechanisms governing ion transport. Dense membranes, typically composed of homogeneous, non-porous polymers, such as Nafion and specialized hydrocarbon ionomers, function primarily via the solution-diffusion mechanism [97]. Ions and solvent molecules dissolve into the polymer matrix at the membrane−electrolyte interface and diffuse through the nanoscale hydrophilic channels formed by the hydrated ionic groups (Fig. 2a). Transport selectivity is achieved predominantly through differences in solubility and diffusivity within this dense polymer phase, coupled with Donnan exclusion effects repelling co-ions of the same charge as the fixed functional groups [98]. This structure inherently creates a significant barrier to bulk electrolyte movement and crossover of active species like vanadium ions, but simultaneously imposes higher ionic resistance due to the tortuous path and limited mobility within the polymer [19].

In contrast, porous membranes possess a distinct, open microstructure defined by a network of interconnected nanopores that extend throughout the entire membrane thickness [99]. Ion transport across these membranes occurs primarily via convective flow and electromigration within electrolyte-filled pores, rather than by dissolution and diffusion through the polymer bulk (Fig. 2b). In porous membranes, selectivity is primarily governed by size-exclusion sieving, with a minor contribution from electrostatic interactions when pore walls are charged, unlike in dense membranes where such interactions are dominant [100]. The pore size distribution is critical: pores must be sufficiently small to physically block the passage of larger active species or their complexes while allowing smaller supporting ions, such as H^+, Cl^-, and SO_4^{2-}, to pass relatively freely. This pore-mediated transport pathway generally results in significantly lower area resistance compared to dense membranes, facilitating higher power density, but creates a more direct conduit for crossover if pore size control or surface charge is inadequate.

This fundamental divergence in transport mechanism leads to the critical performance trade-off central to membrane selection. Dense membranes excel in minimizing active species crossover due to the inherent barrier created by the solution-diffusion process within the dense polymer, crucial for long-term cycling stability and high Coulombic efficiency. However, this comes at the expense of higher ionic resistance, lowering voltage efficiency, and achievable power

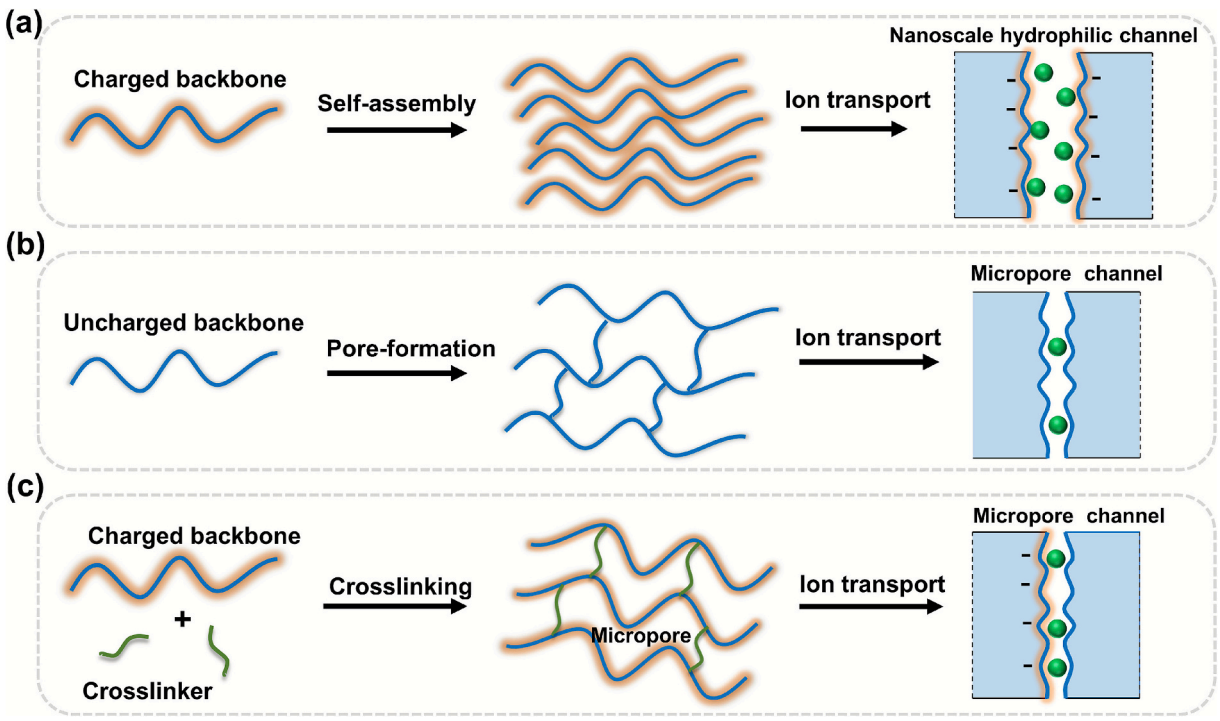

Fig. 2. Schematic illustration of three ion transport mechanisms in RFB membranes: Donnan exclusion in charged dense membranes (a), size sieving in porous membranes (b), and the synergy between the two in charged porous membranes (c).

density. Porous membranes offer the advantage of low ionic resistance and high conductivity, enabling higher power operation, but face a greater challenge in achieving sufficient selectivity. Preventing crossover requires precise engineering of the pore structure (size, tortuosity, and surface charge density) and often relies on electrokinetic effects or the presence of a supporting electrolyte. Impurities and active species can also be more detrimental to porous membrane performance by blocking pores. Hybrid approaches, such as introducing charged functional groups onto porous substrates, aim to combine the low resistance of porous structures with enhanced selectivity approaching that of dense membranes (Fig. 2c) [101–103]. We will have an in-depth discussion on advanced membrane design with different microstructures for next-generation high-performance RFBs in the following section.

3. Advanced membrane design for high-performance RFBs

In this chapter, we present key advancements of functional membrane design for high-performance RFBs, categorized by their microstructural configurations. We first summarize representative examples in dense membranes, including supramolecular-patched Nafion hybrids, nanostructured SPEEK composites, bilayer architectures, and pseudo-nanophase separated PBI systems, which leverage Donnan exclusion and confined transport mechanisms to enhance selectivity and conductivity. Next, we discuss uncharged porous membranes fabricated via methods such as non-solvent induced phase separation (NIPS) and pore-filling techniques, highlighting their reliance on size exclusion for ion selectivity and low resistance. Finally, we examine charged microporous membranes, including functionalized polymers of intrinsic microporosity, hypercrosslinked ion-exchange membranes, and covalent organic framework (COF) composites, which combine tailored pore chemistry and fixed charges to achieve superior ion selectivity and conductivity. These innovations collectively address the conductivity–selectivity–stability trade-offs critical for next-generation RFBs.

3.1. Dense membranes for RFBs

Dense membranes, exemplified by commercial Nafion films, function as critical separators in RFBs, enabling selective ion transport while preventing cross-mixing of redox-active species. Unlike porous membranes relying on size exclusion, dense membranes achieve ion selectivity primarily via electrostatic Donnan exclusion and ion-solvation mechanisms. While previous reviews have systematically examined dense membrane design strategies [10,11], this work does not attempt a comprehensive overview. Instead, we critically assess the most recent representative advances addressing key challenges in dense membranes.

To address the conductivity–selectivity tradeoff, hybridization represents an effective approach in RFB membrane design. As a typical example, Li's group proposed to address the inherent vanadium permeation issue in Nafion membranes by the supramolecular patching strategy [104]. This approach introduces fluorinated block copolymers (FBCs) and polyoxometalates (POMs) as synergistic additives to precisely modify Nafion's ionic nanophase via cooperative noncovalent interactions (Fig. 3a). Unlike conventional hybridization methods that disrupt ionic pathways and sacrifice conductivity, this strategy constructs a contracted (~1 nm) yet continuous ionic network. The modified structure incorporates abundant proton-hopping sites within the shrunk nanodomains while efficiently screening vanadium ions. Consequently, the hybrid membrane exhibits simultaneously enhanced proton conductivity and selectivity.

The same group also developed nanostructured SPEEK hybrid membranes with enhanced ion selectivity for VRFBs [105]. POM-functionalized poly(styrene)-b-poly(vinylpyrrolidone) (PSP) block copolymers are introduced as additives to construct ellipsoidal nanoassemblies (~50 nm) within the SPEEK matrix. These nanostructures are formed by amphiphilic block copolymers, with hydrophobic PS cores imparting vanadium shielding and hydrophilic PVP/POM shells providing abundant proton-hopping sites for efficient proton transport (Fig. 3b). The co-assembly process, driven by multiple noncovalent interactions, integrates proton-conductive nanobarriers without disrupting membrane continuity. Consequently, optimized membranes exhibit

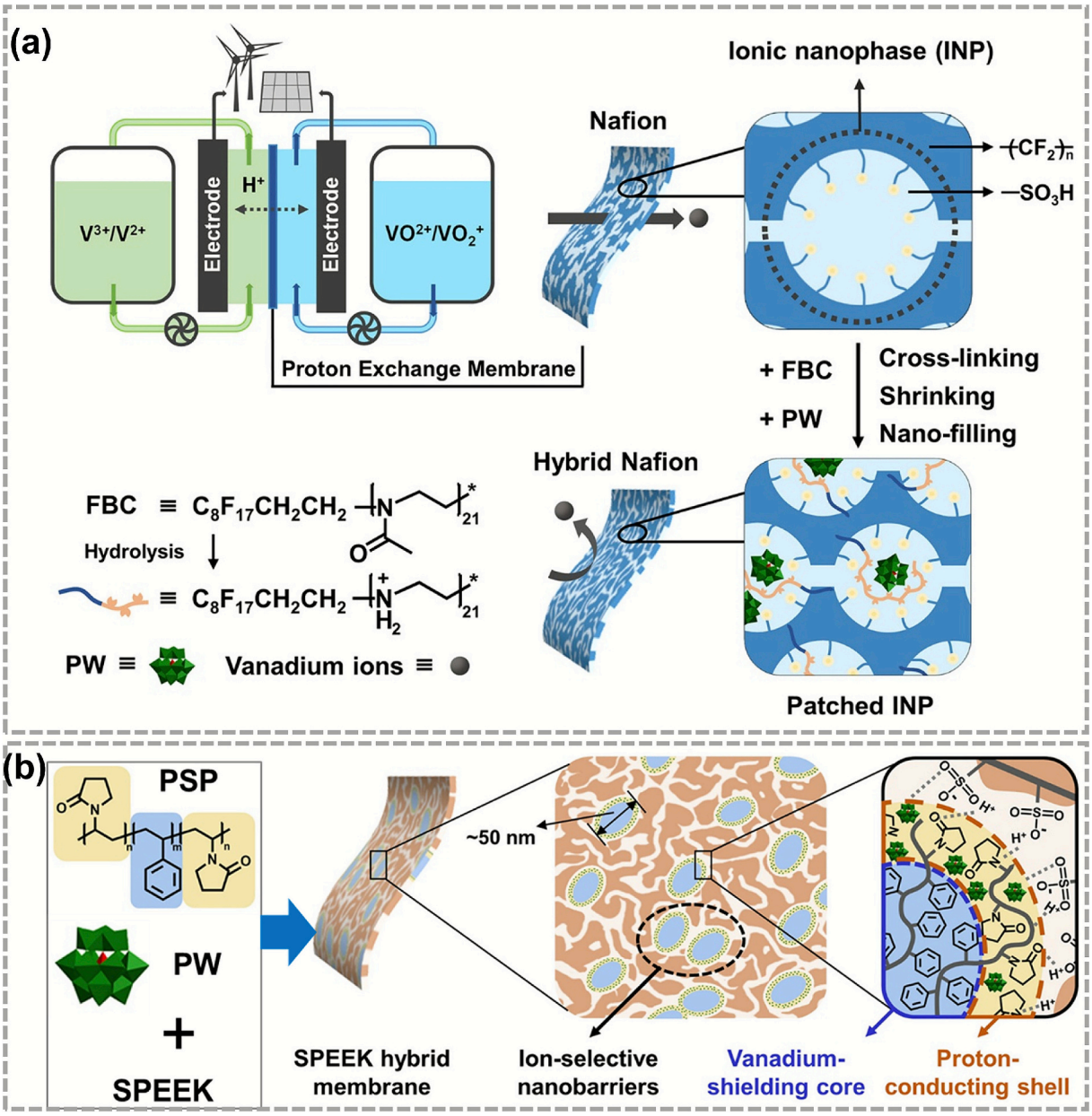

Fig. 3. Hybridization strategies enable high-performance proton-selective RFB membranes. (a) Schematic representation of the synthesis of Nafion/FBC/PW hybrid membranes via an INP-targeted hybridization strategy, and the influence of supramolecular patching effects on membrane fabrication is highlighted. Reproduced with permission from Ref. [104]. Copyright 2023, American Chemical Society. (b) Schematic diagram depicting the self-assembled formation of proton-selective PSP/PW nanobarriers for SPEEK modification. Reproduced with permission from Ref. [105]. Copyright 2023, American Chemical Society.

doubled proton conductivity and reduced vanadium permeability, yielding an eightfold improvement in proton selectivity. Similarly, Wang et al. constructed an advanced composite membrane by incorporating PTFE nanoparticles into an SPEEK matrix using a polydopamine (PDA) bridging layer. The optimized SPEEK/PTFE-0.5 % membrane demonstrated exceptional ion selectivity and significantly improved VRFB performance [106].

Subsequently, various nanophases have been introduced to polymer matrices. Suresh's group fabricated a novel hybrid proton exchange membrane by incorporating hydroxylated boron nitride (OH-BN) into an SPEEK matrix. The OH-BN/SPEEK composite membrane demonstrated significantly enhanced thermal, chemical, and mechanical stability compared to pristine SPEEK. Crucially, it exhibited superior ion selectivity due to reduced vanadium ion permeability while maintaining adequate proton conductivity. Consequently, VRFBs employing this hybrid membrane achieved improved Coulombic efficiency and extended self-discharge time [57]. Sun's group developed a Nafion-based hybrid membrane incorporating superhydrophilic TiO_2 nanotubes, which enhances ion selectivity by obstructing and elongating diffusion pathways, enabling a VRFB to maintain 55.7 % capacity after 1400 cycles [107]. Wang et al. fabricated a hybrid membrane by incorporating sulfonated COFs into a PBI matrix. The functionalized COFs create efficient proton-selective nanochannels, significantly enhancing conductivity while effectively blocking vanadium ion crossover [108].

As an alternative to composite formation, thin films are deposited onto commercial ion-exchange membranes. This approach enhances VRFB performance while maintaining the original battery configuration and operating conditions, utilizing existing commercial membrane sheets. Henkensmeier's group demonstrated that strategically designed

sulfonated polystyrene/PBI bilayer membranes significantly enhance VRFB performance and durability [109]. The optimized PSSP (1–25–25-1) architecture, featuring two stacked bilayers with ultrathin PBI outer layers (1 μm) and conductive sulfonated polystyrene (S42) inner layers (25 μm each), achieves vanadium permeability of 6.85×10^{-14} m^2 s^{-1}, surpassing commercial benchmarks. The enhanced performance is attributed to the synergistic effect of size exclusion and electrostatic repulsion provided by the PBI barriers (Fig. 4a). Critically, the membrane's minimal material cost ($1.84 m^{-2}) positions it as an economically viable alternative to perfluorinated membranes (price of Nafion 212 is in the range of $ 225 m^{-2}). This configuration also maintains a high energy efficiency of 88.5 % while exhibiting substantially reduced area-specific resistance (144.8 mΩ cm^2) in VO^{2+}-containing electrolyte compared to Nafion 212 (439.2 mΩ cm^2). Performance decay observed during extended cycling stems primarily from vanadium crossover and electrolyte imbalance, which was reversible through electrolyte rebalancing, confirming the membrane's intrinsic stability (Fig. 4b). Exceptional operational stability was demonstrated over 3500 cycles (1660 h) at 100 mA cm^{-2} (Fig. 4c). This bilayer design effectively decouples proton conduction (handled by S42) from vanadium blocking (enabled by PBI), offering a scalable strategy for durable, high-efficiency VRFBs.

In another research, Pahlevaninezhad et al. developed electrochemically exfoliated graphene (EEG)-coated Nafion membranes with significantly enhanced performance in VRFBs (Fig. 4d) [25]. As illustrated in Fig. 4e and f, the voltage efficiency (VE) and energy efficiency (EE) of batteries equipped with EEG-coated Nafion 117 and Nafion 115 consistently surpassed those using uncoated membranes throughout cycling. The EEG coating notably improved VE by approximately 10 % for Nafion 117 and 5 % for Nafion 115 at 80 mA cm^{-2}, attributed to reduced electrochemical overpotential despite a marginal increase in area-specific resistance. Consequently, EE increased by up to 13 % relative to bare Nafion membranes. This improvement persisted with minimal degradation after 100 cycles, confirming the coating's electrochemical stability.

Well-defined hydrophilic/hydrophobic nanophase separation has also been extensively employed in RFBs. Conventional approaches

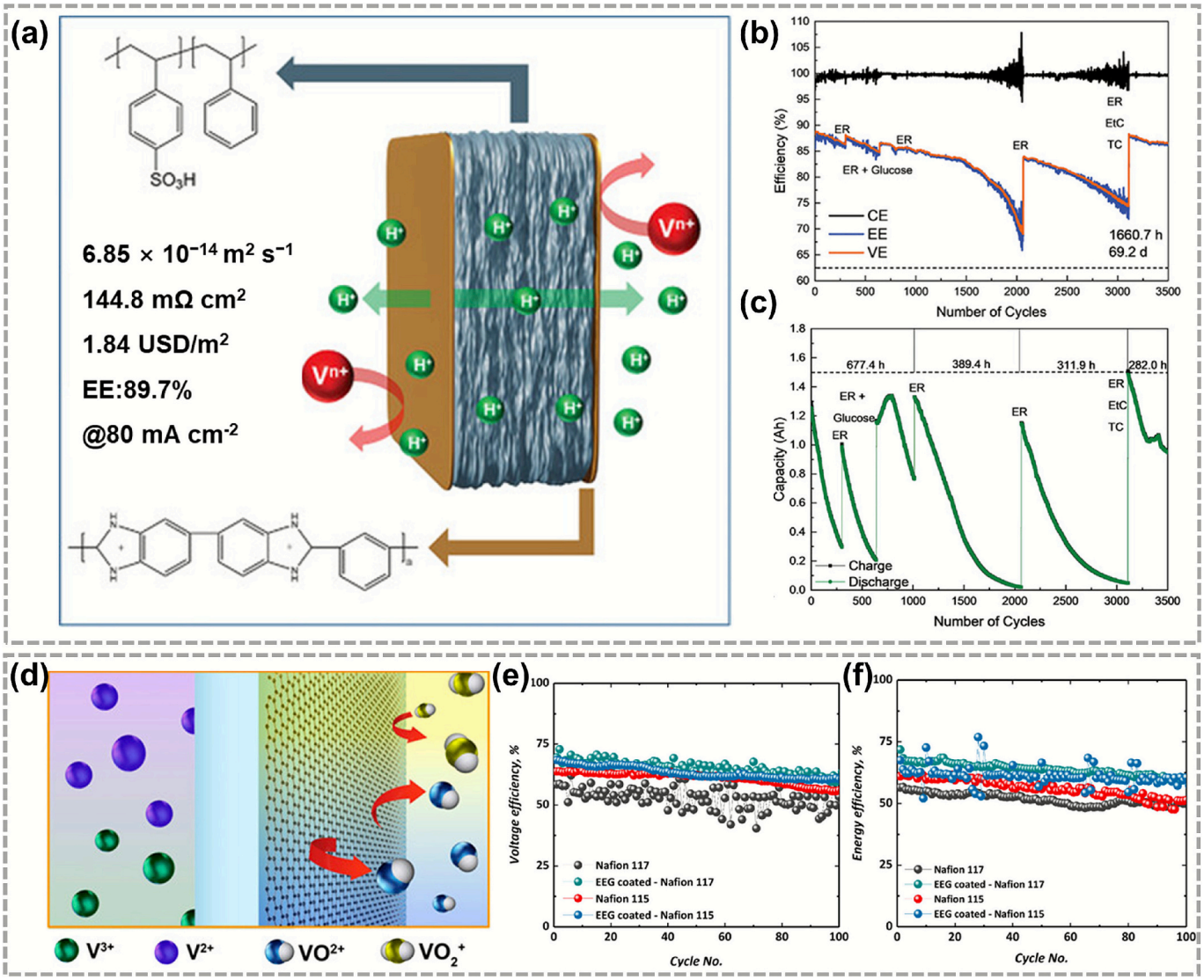

Fig. 4. Novel coating strategies for significantly enhanced battery efficiency and stability. (a) Schematic diagram of the cross-section of PBI-coated sulfonated polystyrene membrane; Efficiency (b) and charge/discharge capacity (c) of PSSP(1–25–25-1) under a constant current density of 100 mA cm^{-2} over 3500 cycles. Reproduced with permission from Ref. [109]. Copyright 2024, Wiley-VCH. (d) Schematic illustration of the working mechanism of ultrathin graphene coatings on Nafion membranes; (e) Cycling performance of the as-fabricated VRFBs, including (e) voltage efficiency (VE), and (f) energy efficiency (EE), evaluated over 100 charge-discharge cycles at a current density of 80 mA cm^{-2} using EEG-coated and uncoated Nafion membranes. Reproduced with permission from Ref. [25]. Copyright 2023, American Chemical Society.

relying on covalently grafted side chains to induce this morphology, however, present synthesis challenges and may compromise membrane stability. Recently, Xiong et al. established a supramolecular-enabled pseudo-nanophase separation strategy for constructing efficient ion-transport highways in polymeric membranes [110]. As illustrated in Fig. 5a, hydrophilic "side chains" are non-covalently grafted onto PBI backbones through multivalent hydrogen-bonding interactions, circumventing covalent modifications that compromise chemical stability. This approach spontaneously induces microphase separation during membrane formation, generating interconnected hydrophilic nanochannels (3–14 nm). Following electrolyte infusion, these channels enable rapid proton transport via a bulk-like conduction mechanism (Fig. 5b), contrasting sharply with the restricted hopping mechanism observed in unmodified PBI membranes. These characteristics translate to superior VRFB performance. Membranes exhibit near-unity Coulombic efficiency (99.5–100 %) across current densities of 40–300

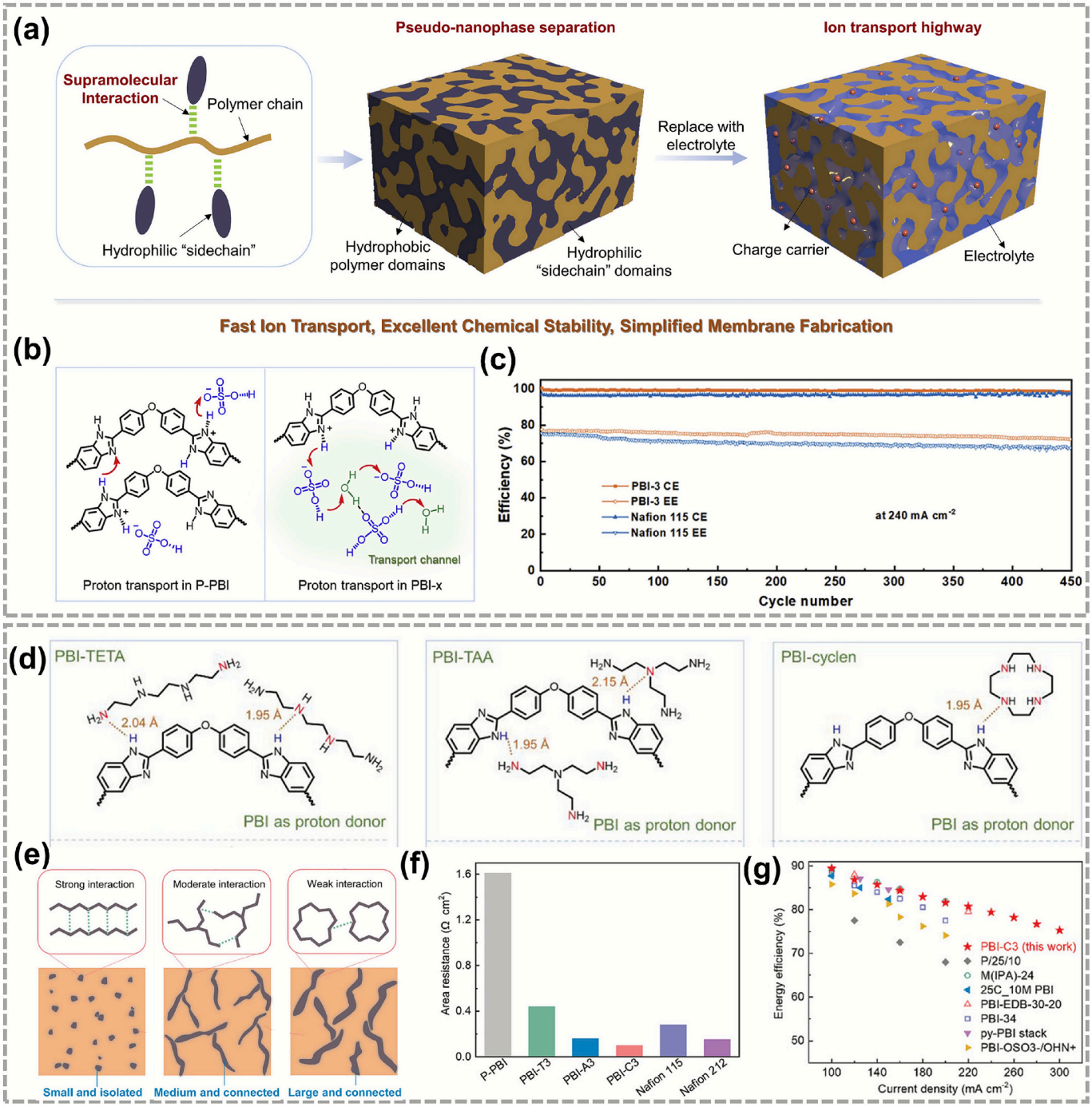

Fig. 5. Thin films depositing onto commercial ion-exchange membranes for boosted RFB performances. (a) Schematic representation of ion-transport highway formation via pseudo-nano-phase separation mediated by supramolecular interactions. (b) Schematic depiction of proposed proton conduction pathways through the Grotthuss mechanism in P-PBI and PBI-x membranes. (c) Cycling efficiency of VRFBs assembled with PBI-3 and Nafion 115 membranes at the current density of 240 mA cm^{-2}. Reproduced with permission from Ref. [110]. Copyright 2024, Elsevier. (d) PBI-amine hydrogen bonding types. (e) Mechanism of membrane microstructure alteration by supramolecular sidechain topology. (f) PBI-based vs. Nafion membrane area resistance. (g) EE comparison of PBI-based vanadium RFBs and PBI-C3 RFB (this work). Reproduced with permission from Ref. [111]. Copyright 2024, Wiley-VCH.

mA cm^{-2} due to the effective Donnan exclusion. Critically, the VRFB assembled with optimized membranes (PBI-3) demonstrates remarkable cycling stability over 450 cycles at 240 mA cm^{-2} (Fig. 5c).

Subsequently, the same group grafted three topological variants, i.e., linear (TETA), branched (TAA), and cyclic (cyclen) amines, non-covalently onto PBI backbones via comparable hydrogen-bonding strengths (Fig. 5d), yet induced distinct microstructural morphologies [111]. As shown in Fig. 5e, linear TETA's strong intermolecular interactions promote tight packing, yielding small (~5 nm) but isolated hydrophilic domains. Conversely, cyclic cyclen's weak self-interaction enables loose molecular stacking, forming larger (~12 nm) interconnected channels, while branched TAA exhibits intermediate behavior. These topological effects directly govern ion transport: cyclic-topology membranes achieve a low area resistance of 0.10 Ω cm^2 (Fig. 5f), surpassing Nafion 212 by 33 % due to optimized proton highways. Moreover, cyclen-mediated membranes deliver a high energy efficiency of 80.7 % even at 220 mA cm^{-2} (Fig. 5g).

The widespread commercialization of RFBs is limited by high costs and performance issues, notably the poor chemical stability and insufficient ion selectivity of current commercial Nafion membranes, as well as their fluorinated composition. This challenge is further intensified by imminent regulatory restrictions, including forthcoming EU prohibitions on PFAS by the early 2030s [112]. Non-fluorinated membranes that include highly acidic sulfonic acid groups within hydrocarbon matrices serve as effective alternatives to PFAS-based systems. As a typical example, Henkensmeier's group fabricated dense, fluorine-free sulfonated para-polybenzimidazole (MS-PBI) membranes with exceptional performances in VRFBs (Fig. 6a) [87]. As illustrated in Fig. 6b, Coulombic efficiency (CE) exhibits an inverse relationship with temperature, decreasing from 99.7 % at 25 °C to 98.7 % at 35 °C (80 mA cm^{-2}, MS-PBI #1 membrane) due to enhanced vanadium ion mobility at elevated temperatures. Conversely, energy efficiency (EE) benefits significantly from higher temperatures under high-current-density operation (Fig. 6c). For example, at 300 mA cm^{-2}, EE reaches 80.3 % at 35 °C, compared to only 72.3 % at 25 °C. This improvement is attributable to reduced ohmic losses from improved proton conductivity. At lower current densities (80 mA cm^{-2}), EE remains consistently high, exceeding 92 % across different temperatures, which indicates minimal sensitivity to temperature changes. Long-term cycling tests (Fig. 6d) further confirm the durability of the system, with EE retention exceeding 98 % after 100 cycles at 80 mA cm^{-2} and minimal capacity fade (27 % loss at 25 °C). Khataee's group fabricated a series of poly (terphenylene) membranes incorporating zwitterionic (sulfoalkylated piperidinium) and cationic (piperidinium) moieties at controlled ratios (40–60 %). The as-assembled VRFBs with the zwitterionic membranes exhibited comparable performance to Nafion 212 in key metrics, including ionic conductivity, capacity retention, and chemical stability [113].

3.2. Porous membranes for RFBs

Porous membranes represent a distinct class of separators for RFBs, leveraging size-sieving mechanisms rather than electrostatic interactions to achieve ion selectivity [20]. Unlike dense ion-exchange membranes, porous membranes physically block larger hydrated vanadium ions while permitting smaller charge-balancing ions to traverse their nanopores. This section reviews recent advances in porous membrane design for VRFBs, focusing on different approaches for constructing the porous structure.

As a typical example, NIPS was introduced as a versatile and scalable fabrication method for designing porous carbon electrodes tailored for RFBs [114]. As demonstrated in Fig. 7a, the process involves casting a polymer solution containing polyacrylonitrile (PAN) and poly(vinylpyrrolidone) (PVP), followed by immersion in a non-solvent bath to induce phase separation. Subsequent drying, thermal stabilization, and carbonization yield mechanically robust, electrically conductive

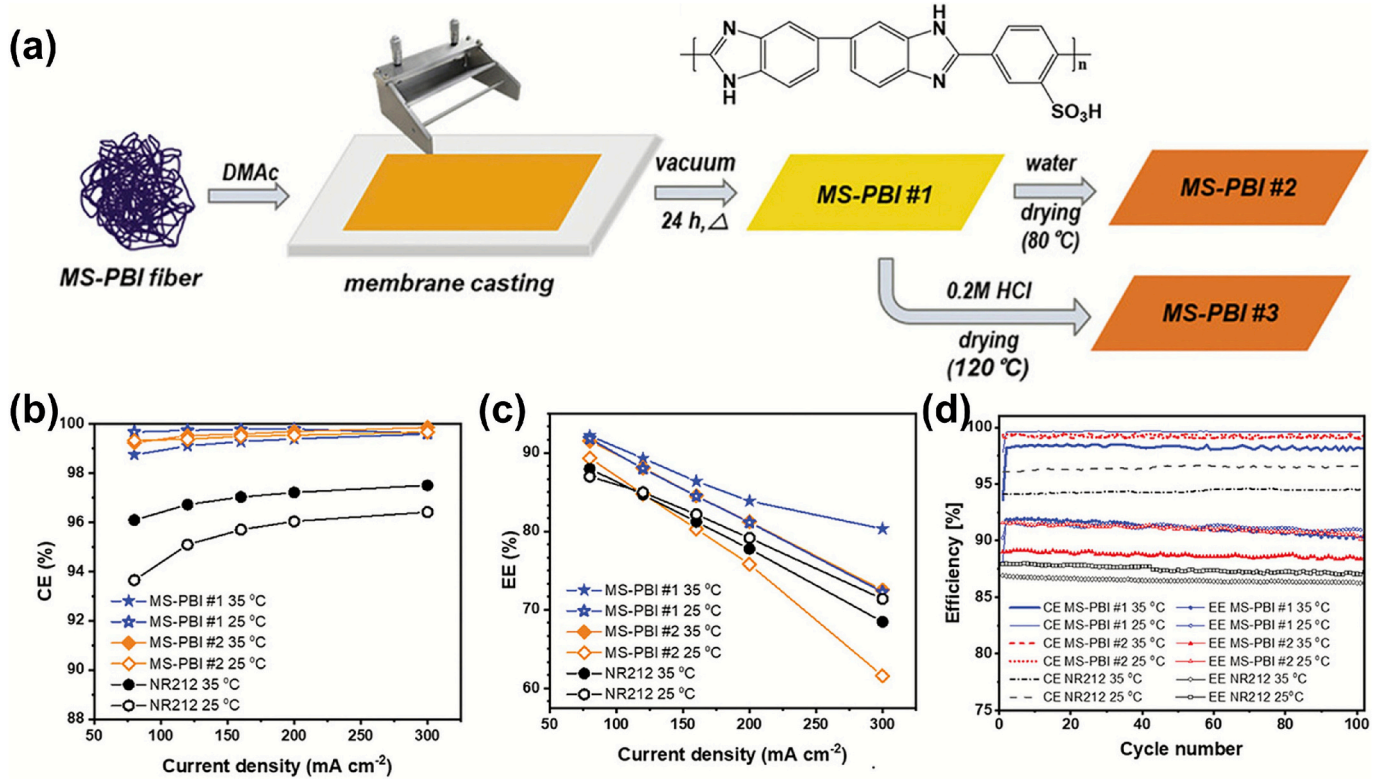

Fig. 6. Non-fluorinated membranes incorporating highly acidic sulfonic acid groups within hydrocarbon matrices for RFBs. (a) Molecular design and fabrication of MS-PBI membranes. VRFB performance of CE (b) and EE (c) with NR212, MS-PBI #1, and MS-PBI #2 membranes, respectively, at 25/35 °C and current densities of 80–300 mA cm^{-2}. (d) Cycling performances of MS-PBI #1 and #2 at 80 mA cm^{-2}. Reproduced with permission from Ref. [87]. Copyright 2024, Wiley-VCH.

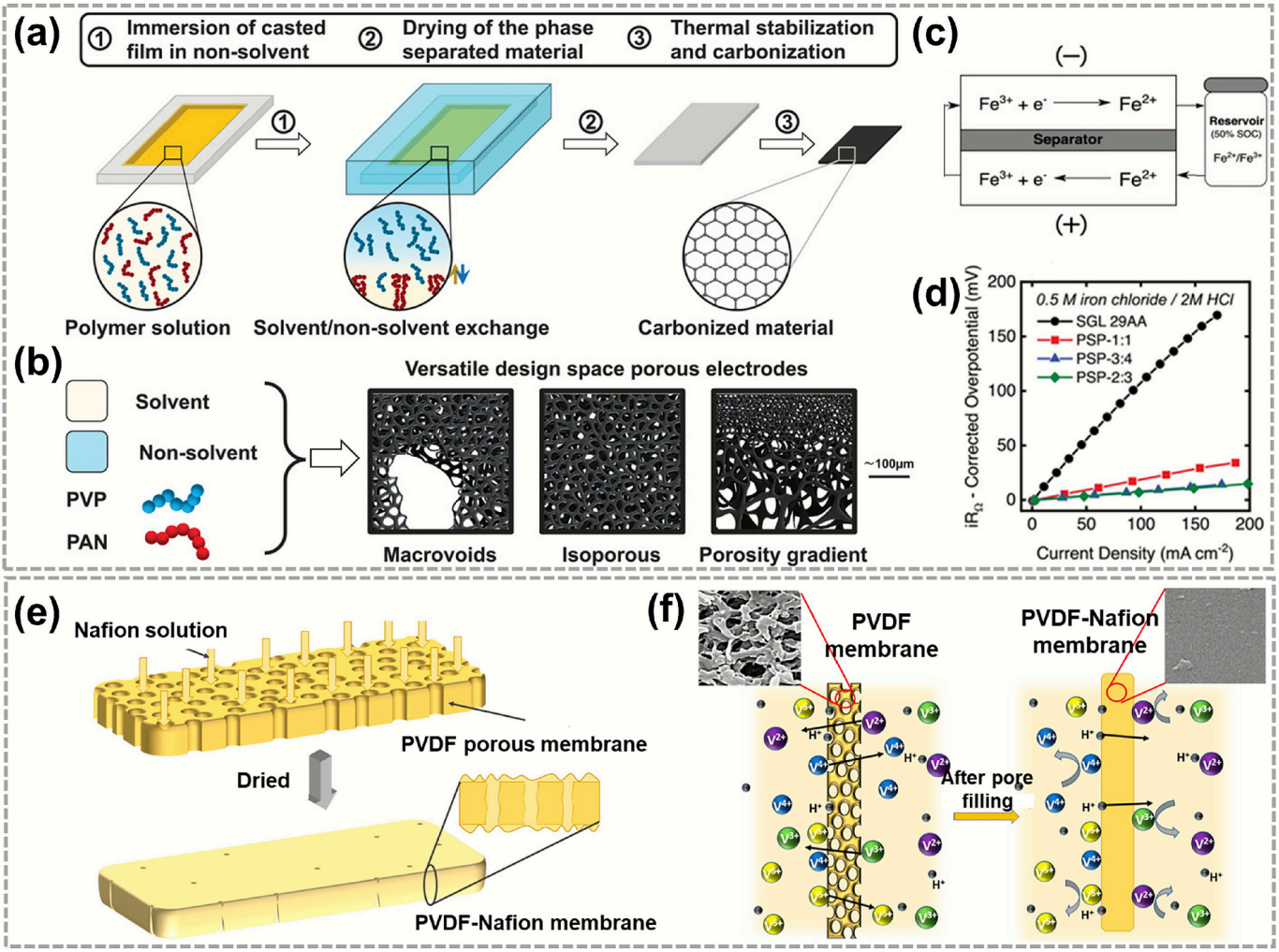

Fig. 7. NIPS for versatile and scalable fabrication of porous membranes. (a) Schematic of the phase separation process for fabricating flat carbon sheets. (b) Spectrum of porous microstructures accessible via the NIPS technique, with representative examples illustrated (right). (c) Schematic of the single-reservoir, iron chloride electrolyte setup. (d) Polarization curves measured at 5 cm s^{-1} for SGL 29AA and PSP variants (1:1, 3:4, 2:3). Reproduced with permission from Ref. [114]. Copyright 2021, Wiley-VCH. (e) Fabrication of the PVDF–Nafion membrane via the pore-filling method. (f) Operational principle of the pore-filled PVDF–Nafion composite. Reproduced with permission from Ref. [115]. Copyright 2023, American Chemical Society.

electrodes with hierarchical porosity. Fig. 7b highlights the tunability of the microstructure through easily adjustable parameters, such as polymer composition, which enables the creation of multimodal pore networks, including gradient and isotropic structures. Electrochemical performance was evaluated using a single-electrolyte flow cell with an iron chloride redox couple (Fig. 7c). Polarization curves (Fig. 7d) demonstrated that NIPS-derived electrodes exhibit reduced overpotentials and improved current densities compared to conventional carbon electrodes, attributed to their hierarchical pore structure, which enhances mass transport and surface accessibility.

In another research, Verma's group fabricated a low-cost pore-filled composite membrane by impregnating a porous PVDF substrate with Nafion solution [115]. As illustrated in Fig. 7e, the synthesis involves pretreatment of the PVDF membrane, followed by drop-casting of Nafion solution, solvent evaporation, and thermal drying, resulting in uniform filler distribution within the pores. The incorporated Nafion forms a tortuous pathway that significantly hinders vanadium ion crossover (Fig. 7f). Although proton conductivity is somewhat compromised, the composite membrane exhibits notable economic advantages and reduced self-discharge, demonstrating strong potential as a cost-effective and durable alternative to conventional Nafion membranes in VRFBs.

Membranes with inherent micro- or nanopores circumvent the need for artificial pore generation, thereby simplifying the fabrication process [117]. Furthermore, such intrinsic pores often exhibit uniform size and are tunable at the nanometric or sub-nanometric scale, with a narrow distribution of pore sizes. This inherent regularity alleviates the difficulties associated with controlling membrane morphology. For instance, Li's group developed a thin-film composite membrane (TFCM) with an ultrathin polyamide selective layer, designed to address the long-standing trade-off between ion conductivity and selectivity [116]. As shown in Fig. 8a, the membrane was fabricated via interfacial polymerization of trimesoyl chloride (TMC) and *m*-phenylenediamine (MPD), resulting in a continuous and defect-free selective layer that exhibits a characteristic "ridge-and-valley" morphology (Fig. 8b). This layer has a thickness of approximately 40 nm and is supported by a porous substrate (Fig. 8c). Ab initio molecular dynamics (AIMD) simulations revealed that the polyamide layer contains sub-1 nm pores (Fig. 8d), which facilitate proton transport through both Vehicle (Fig. 8e) and Grotthuss (Fig. 8f) mechanisms. Additionally, these pores effectively exclude larger hydrated vanadium ions through size exclusion. This unique structure enables exceptionally high proton conductivity and selectivity. Battery performance tests demonstrated that a VFB equipped with this membrane achieved an energy efficiency exceeding

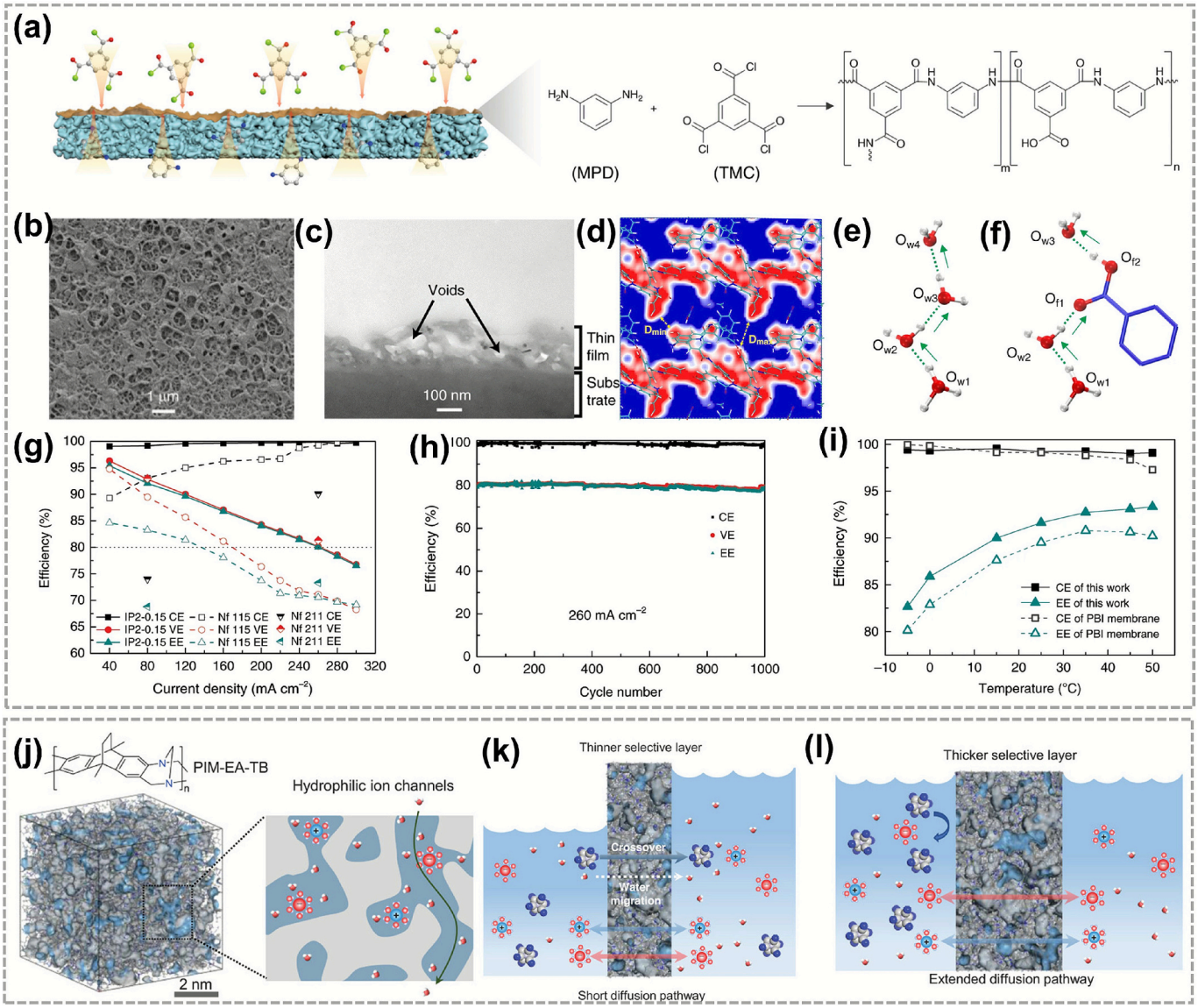

Fig. 8. Membranes with intrinsic pores for optimized ion conductivity and selectivity. (a) Mechanism schematic of interfacial polymerization. (b) Surface morphology of IP2–0.15. (c) Cross-sectional TEM image of IP2–0.15. (d) 2D channel structure parallel to the y and z-axes, with the accessible area in blue and the framework (inaccessible area) in red. (e) Water-mediated transfer. Atoms: O(red), H(white). (f) Transfer through carboxyl groups and water. Atoms: O(red), C(blue), H(white). (g) Efficiencies of IP2–0.15 vs. Nafion 115 membranes at different current densities. (h) Cycling performance of the IP2–0.15 system at a current density of 260 mA cm^{-2}. (i) Efficiencies of IP2–0.15 vs. prior high-performance porous PBI membrane. Reproduced with permission from Ref. [116]. Copyright 2020, Springer Nature. (j) 3D visualization of an amorphous PIM-EA-TB membrane from the authors' earlier study, along with a schematic illustration of its water-mediated hydrophilic ion channels. (k) Significant net volume change in an RFB employing a thin selective membrane. (l) Controlled net volume change in an RFB utilizing a thicker selective membrane. Reproduced with permission from Ref. [50]. Copyright 2023, Wiley-VCH. (For interpretation of the references to colour in this figure legend, the reader is referred to the web version of this article.)

80 % even at a current density of 260 mA cm^{-2} (Fig. 8g), along with outstanding cycling stability and minimal capacity decay over 1000 cycles (Fig. 8h). The membrane also exhibited robust performance across a wide temperature range, underscoring its potential for high-power-density, durable flow battery applications (Fig. 8i).

Similarly, Tan et al. proposed to regulate mass transport through the use of TFCM based on Tröger's base polymer of intrinsic microporosity (PIM-EA-TB) [50]. The membrane features well-defined hydrophilic ion channels that facilitate selective ion conduction (Fig. 8j). It is noteworthy that severe net volumetric electrolyte transfer occurs in RFBs equipped with thinner selective layers, which leads to significant water migration and crossover of redox species (Fig. 8k). In contrast, employing a thicker selective layer, as depicted in Fig. 8l, effectively mitigates these transport issues, resulting in managed electrolyte transfer and enhanced operational stability. By optimizing the thickness of the PIM-EA-TB selective layer, the crossover of redox-active species is reduced by 1–2 orders of magnitude, and water migration is significantly suppressed, thereby prolonging the cycling life of RFBs with minimal capacity fade.

In addition to polymers of intrinsic microporosity, research interest has expanded to other intrinsically porous materials, such as COFs and metal–organic frameworks (MOFs), for membrane applications, owing to their tunable pore channels, ion selectivity, and structural design flexibility [118]. Recently, acid-stable zirconium-based MOFs, namely MOF-801 and MOF-808, were incorporated as functional fillers into an SPEEK matrix to fabricate advanced RFB membranes [119]. The distinct pore architectures of these MOFs, i.e., triangular windows (~3.5 Å) in MOF-801 and larger hexagonal apertures (~10.1 Å) in MOF-808, enable

tailored ion-sieving properties and proton-conduction pathways (Fig. 9a). Molecular MOF-801's sieving effect effectively suppresses vanadium ion crossover. At the same time, the highly interconnected and protophilic channels of MOF-808 facilitate rapid proton transport. Consequently, electrochemical performance evaluations revealed that the composite membrane with MOF-801 (S/801–3) exhibited superior Coulombic efficiency, reaching 98.5–99.2 % across current densities of 40–120 mA cm^{-2} (Fig. 9b). In contrast, the MOF-808-incorporated membrane (S/808–3) demonstrated significantly enhanced voltage efficiency values of 93.7–84.1 % (Fig. 9c). The critical role of MOF pore geometry in balancing ion selectivity and conductivity is thus underscored.

Subsequently, Huang's group engineered hollow MOFs with graded lattice defects to construct high-performance ion-conducting membranes [120]. They selectively etched the internal defective core of MIL-101 under acidic conditions to produce hollow HMIL-101. This new

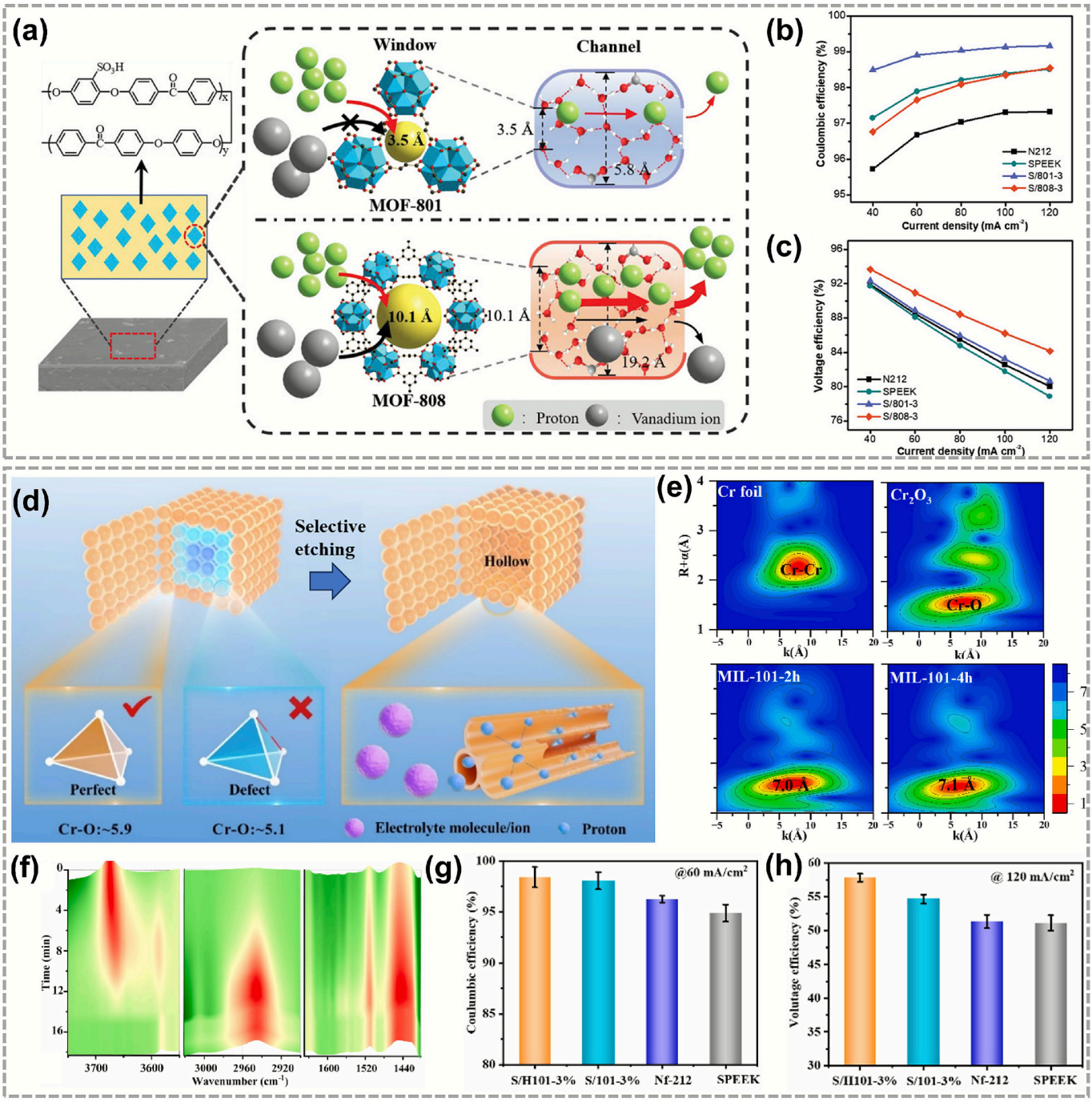

Fig. 9. Fabrication of COFs/MOFs-based membranes for high-performance RFBs. (a) Schematic of a SPEEK-based composite incorporating acid-stable Zr-MOF fillers with tunable pore structures. Efficiency comparison of VRFBs employing N212, SPEEK, S/801–3, and S/808–3 membranes: (b) CE and (c) VE at increasing current densities ranging from 40 to 120 mA cm^{-2}. Reproduced with permission from Ref. [119]. Copyright 2023, Wiley-VCH. (d) Schematic of hollow MIL-101 (HMIL-101) equipped with ultralow-resistance internal transport channels and a lattice-perfect outer shell for ion sieving, constructed via a lattice difference strategy. (e) Comparative analysis of the Cr K-edge wavelet-transform EXAFS spectra for MIL-101-2 h, MIL-101-4 h, Cr foil, and Cr_2O_3. (f) In situ TG-IR-MS analysis of fully hydrated HMIL-101 within a specific range. (g) Coulombic efficiency (CE) and (c) voltage efficiency (VE) of cells with various membranes measured at current densities of 60 and 120 mA cm^{-2}, respectively. Reproduced with permission from Ref. [120]. Copyright 2025, Elsevier.

structure features an ultralow-resistance internal reservoir channel, which is surrounded by a lattice-perfect ion-sieving shell (Fig. 9d). Synchrotron X-ray absorption fine structure (XAFS) spectroscopy quantitatively revealed a gradient in Cr—O coordination numbers from the defective core (~5.1) to the nearly perfect shell (~5.9), confirming the presence of structurally distinct regions (Fig. 9e). The resulting cavity significantly enhanced proton transport, with proton conductivity increasing by nearly an order of magnitude (2.9×10^{-3} vs. 4.0×10^{-4} S cm^{-1}) due to near-frictionless diffusion within the hydrated reservoir, as supported by in situ thermogravimetric-infrared analysis accompanied by mass spectroscopy (TG-IR-MS) (Fig. 9f). When incorporated into a SPEEK matrix, the HMIL-101-based membrane demonstrated exceptional performance in AORFBs, achieving a Coulombic efficiency exceeding 97 % at 60 mA cm^{-2} (Fig. 9g) and a voltage efficiency of 57.4 % at 120 mA cm^{-2}, 7 % higher than that of a commercial Nafion-212 membrane (Fig. 9h).

3.3. Charged microporous membranes for RFBs

By strategically incorporating charged functional groups into porous substrates, charged microporous membranes harness the inherently low ionic resistance of porous architectures while attaining selectivity levels comparable to those of dense membranes. Through precise control over pore chemistry and the introduction of fixed charged sites, these modified membranes achieve a synergistic enhancement in both ion selectivity and conductivity, effectively overcoming the traditional trade-off between these critical performance parameters [102,121,122].

For instance, Song's group developed a series of ion-sieving sulfonated polymer membranes based on a microporous spirobifluorene-derived polymer (PIM-SBF) for aqueous organic RFBs [123]. The membranes were functionalized with sulfonate groups via a controlled reaction using trimethylsilyl chlorosulfonate. This process allowed for precise tuning of the ion exchange capacity while preserving the microporous structure. As illustrated in Fig. 10a, b, the rigid and contorted polymer backbone facilitates the formation of subnanometer channels that promote selective ion transport. The relationship between ionic conductivity and ferrocyanide permeability is illustrated in the upper-bound plot (Fig. 10c). This plot demonstrates that the optimized membrane (sPIM-SBF-1.40) surpasses commercial benchmarks such as Nafion 115, offering a favorable balance between high ionic conduction and effective rejection of redox-active species. Electrochemical tests using electrolytes at pH 9 revealed that cells equipped with sPIM-SBF membranes exhibit enhanced energy efficiency across various current densities (Fig. 10d) and significantly improved cycling stability, with a capacity decay rate as low as 0.0335 % per day over 2100 cycles, outperforming Nafion-based cells by two orders of magnitude (Fig. 10e).

More recently, the same group fabricated ion-selective membranes for RFBs through the physical blending of carboxylate-functionalized (cPIM-1) and amidoxime-functionalized (AO-PIM-1) polymers of intrinsic microporosity [124]. As illustrated in Fig. 10f, the two functional polymers form a microscopically homogeneous and interpenetrating network facilitated by strong cohesive interactions, including hydrogen bonding and salt-bridge formation between carboxylic acid and amidoxime groups. This stands in sharp contrast to the macroscopic phase separation observed in control blends of cPIM-1 with unfunctionalized PIM-1. The incorporation of ionizable groups within the sub-nanometer pores enables tunable ion-transport properties, while the rigid polymer backbones restrict excessive swelling and provide molecular-sieving functionality. The resulting blend membranes achieve an optimal balance between high ionic conductivity and exceptional selectivity against crossover of redox-active species, significantly outperforming commercial Nafion membranes.

Recently, Wong et al. incorporated three-dimensional triptycene units into the polymer backbone to overcome the performance limitations of conventional SPEEK membranes [125]. The contorted triptycene structures disrupt chain packing and generate intrinsic microporosity, forming highly interconnected, hourglass-shaped subnanometer channels that facilitate efficient dual ion transport (Fig. 11a-d). These engineered membranes exhibit significantly enhanced ionic conductivity, particularly for hydroxide ions in alkaline media, due to continuous hydrogen-bonding networks enabling Grotthuss-type conduction, while maintaining exceptional molecular sieving selectivity against redox-active species. When integrated into neutral pH aqueous organic RFBs, the optimized sPEEK-Trip-1.55 membrane substantially improved energy efficiency, achieving over 80 % at 100 mA cm^{-2} (Fig. 11e), and supported stable long-term cycling with minimal capacity decay (Fig. 11f). The unique microporous architecture effectively decouples the traditional trade-off between conductivity and selectivity, positioning these membranes as promising enablers for high-power, durable flow battery systems.

Xu's group developed a facile hypercrosslinking strategy to transform conventional quaternized polyphenylene oxide (QPPO) membranes into microporous ion exchange membranes (HC-QPPO) for application in pH-neutral aqueous organic RFBs [101]. As illustrated in Fig. 11g, the hypercrosslinking process involves a simple Friedel–Crafts alkylation reaction, which introduces a rigid microporous framework while retaining the original charged functionalities. The resulting HC-QPPO membrane exhibits significantly enhanced performance: ionic conductivity more than doubles (Fig. 11h), and selectivity is improved by over an order of magnitude (Fig. 11i), effectively overcoming the typical conductivity–selectivity trade-off. When deployed in a flow battery, the HC-QPPO membrane demonstrates markedly reduced area-specific resistance and exceptional cycling stability, with a capacity fade rate as low as 0.0017 % per cycle (Fig. 11j). This approach combines the commercial availability of traditional membranes with the performance advantages of microporous polymers, thus offering a promising pathway toward high-performance, cost-efficient energy storage devices.

Functionalized COF that have a high density of functional groups offer promising potential for exceptional proton conductivity and remarkable stability in high-performance RFBs. However, creating functionalized COF membranes that achieve both high ion selectivity with robust durability remains a significant challenge. Recently, Jiang's group successfully developed a hybrid proton exchange membrane by incorporating sulfonated COF into an SPEEK matrix [126]. As illustrated in Fig. 12a, the well-defined nanochannels and high density of $–SO_3H$ groups in SCOF facilitate efficient proton transport via both Grotthuss and vehicle mechanisms. The hybrid membrane exhibits significantly reduced vanadium ion permeability (Fig. 12b) and enhanced proton conductivity, culminating in superior ion selectivity (Fig. 12c). When evaluated in a VRFB single cell, the SCOF/SPEEK membrane achieves higher Coulombic efficiency and energy efficiency across various current densities compared to Nafion212 and pristine SPEEK membranes (Fig. 12d, e). Moreover, it demonstrates outstanding capacity retention after 200 cycles (Fig. 12f).

In another research, Wang et al. incorporated an ionic covalent organic polymer (iCOP) into a Nafion matrix to fabricate a composite proton exchange membrane for iron-chromium RFBs [127]. As depicted in Fig. 12g, the iCOP was synthesized via interfacial polymerization and integrated into the membrane to provide abundant sulfonic acid groups and protonated amine functionalities. These features facilitate the formation of efficient proton transport pathways through a hydrogen-bond network while simultaneously suppressing the crossover of Fe^{3+} and Cr^{3+} ions via the Donnan exclusion effect. The iCOP-8 membrane (with 0.8 wt% iCOP) exhibited outstanding battery performance, achieving

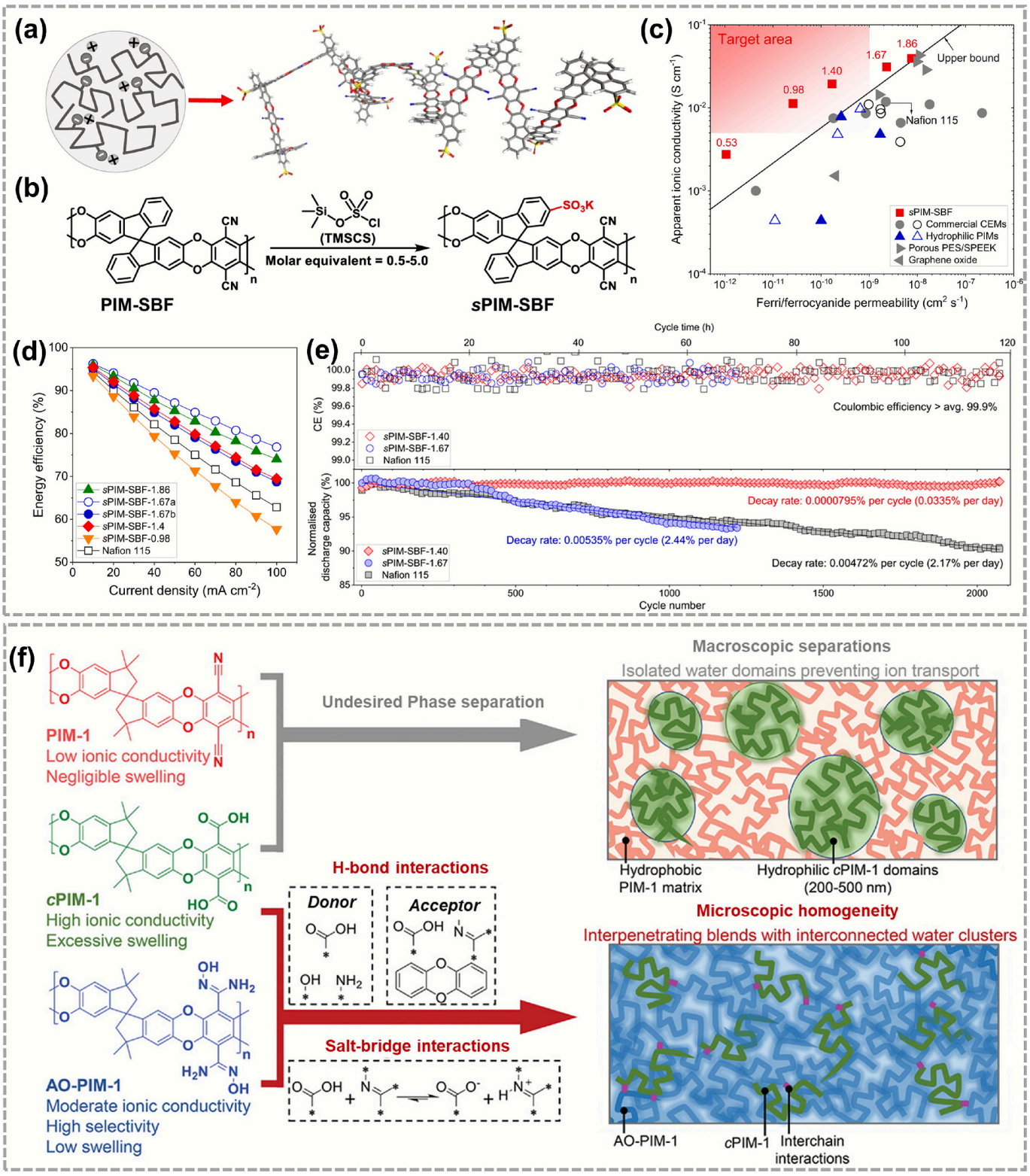

Fig. 10. Charged microporous polymer design for simultaneously high conductivity and selectivity. (a) Molecular model and schematic of a rigid, contorted polymer chain with sulfonate groups in a PIM. (b) Synthesis pathway for sPIM-SBF. (c) Upper bound of ferri/ferrocyanide permeability vs. apparent ionic conductivity. (d) Energy efficiency versus current density (10–100 mA cm^{-2}) for membranes of various thicknesses: Nafion 115 (142 μm), sPIM-SBF-1.86 (176 μm), sPIM-SBF-1.67a (45 μm), sPIM-SBF-1.67b (177 μm), sPIM-SBF-1.40 (134 μm), and sPIM-SBF-0.98 (139 μm). (e) Cycling performance at the current density of 100 mA cm^{-2} and pH of 9 for RFBs using sPIM-SBF-1.40 (134 μm), sPIM-SBF-1.67b (177 μm), and Nafion 115 membranes, with linearly fitted capacity decay rates. Tests were conducted at ~30 °C. Reproduced with permission from Ref. [123]. Copyright 2022, Springer Nature. (f) Chemical structures and morphology of PIM-1, cPIM-1, and AO-PIM-1. Reproduced with permission from Ref. [124]. Copyright 2023, Wiley-VCH.

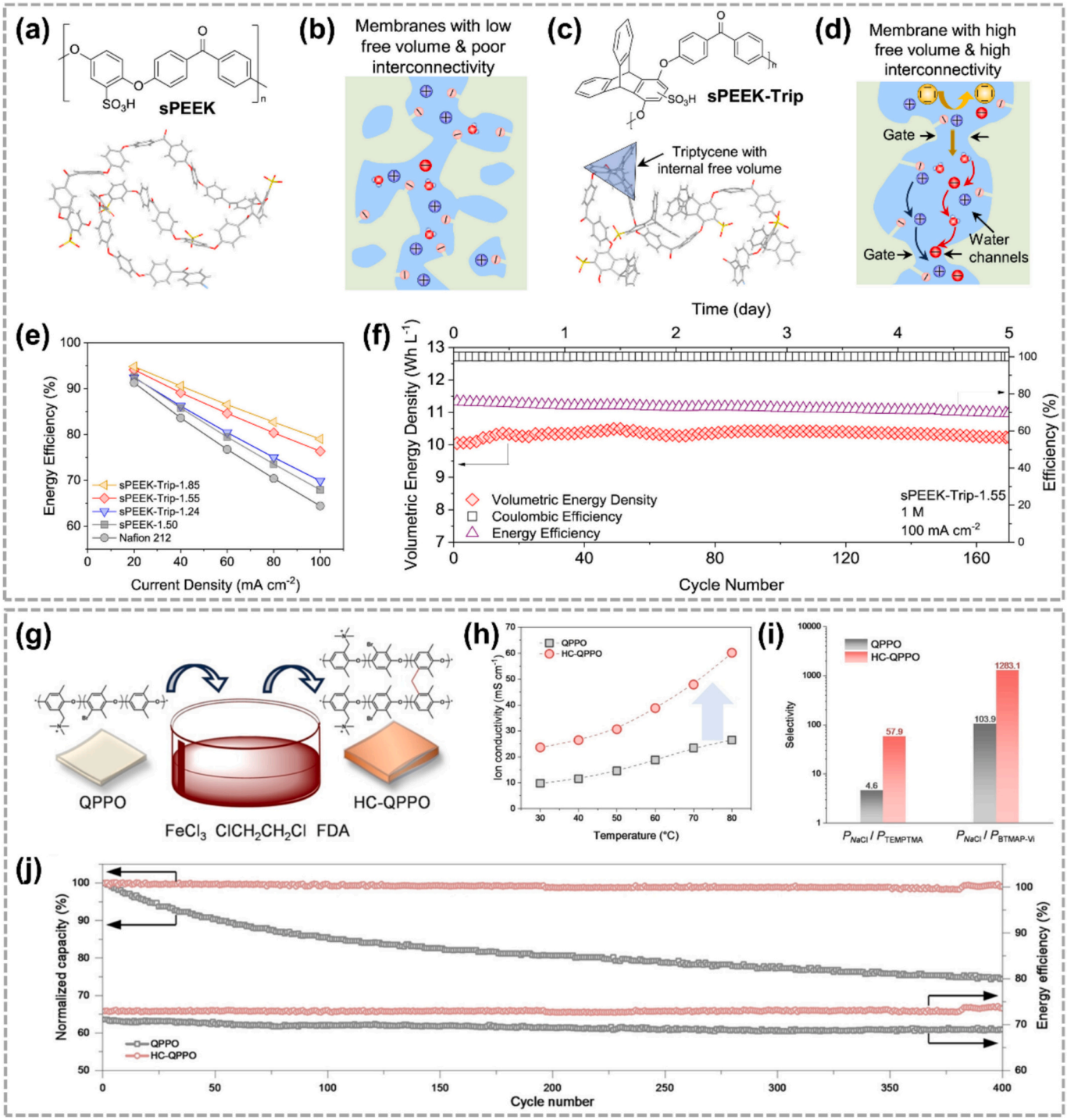

Fig. 11. Novel microstructure design breaks ion transport trade-offs in RFB membranes. (a) Chemical structure and chain segment of conventional sPEEK. (b) Ion channel morphology of sPEEK membranes. (c) Chemical structure of sPEEK-Trip, featuring triptycene units that create internal free volume. (d) Hourglass-shaped interconnected ion channels in sPEEK-Trip membranes, enabling fast and selective transport of both cations (black arrows) and hydroxide ions (red arrows) in alkaline media. (e) Energy efficiency versus current density (20–100 mA cm^{-2}). (f) Galvanostatic cycling at the current density of 100 mA cm^{-2} of a $Na_4/K_4[Fe(CN)_6]$ | $(SPr)_2V$ cell using sPEEK-Trip-1.55 membrane. Reproduced with permission from Ref. [125]. Copyright 2025, Elsevier. (g) Schematic of the hypercrosslinking process: from linear polymer to proposed network structure. (h) Ionic conductivity of QPPO and HC-QPPO membranes at varied temperatures, measured in 1.0 M NaCl; (i) Selectivity toward redox-active species, represented by PCl−/PBTMAP-Vi and PCl−/PTEMPTMA. (j) Normalized capacity and energy efficiency versus cycle number for 0.1 M cells with QPPO and HC-QPPO membranes at 100 mA cm^{-2}. Reproduced with permission from Ref. [101]. Copyright 2024, Wiley-VCH. (For interpretation of the references to colour in this figure legend, the reader is referred to the web version of this article.)

high CE and EE across a range of current densities (Fig. 12h, i). Specifically, it reached a CE of 97.66 % and an EE of 87.11 % at 100 mA cm^{-2}, significantly outperforming the recast Nafion membrane.

To facilitate a direct comparison of the properties and performances of the state-of-the-art membranes discussed in this section, summary tables are provided below. Table 3 summarizes key membrane properties including thickness, swelling behavior, ion transport characteristics, and selectivity metrics, while Table 4 provides performance data under

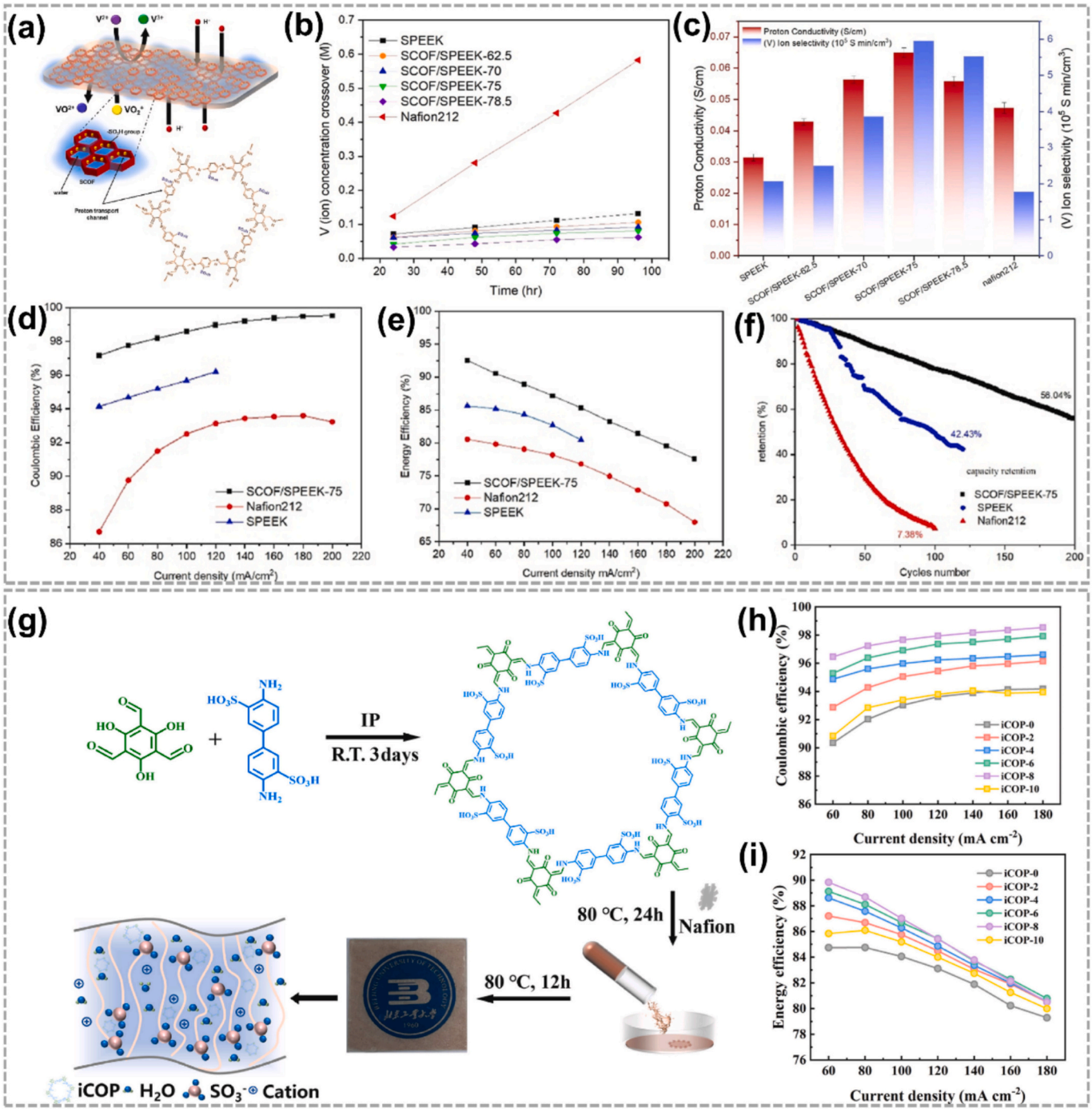

Fig. 12. Functionalized COFs-based membranes enable high-performance, durable RFBs. (a) Schematic of proton-selective transport in SCOF/SPEEK membranes; (b) Vanadium ion permeability; (c) Proton conductivity and ion selectivity of SPEEK and SCOF/SPEEK. (d) CE, (e) VE, and (f) Discharge capacity retention at 100 mA cm^{-2} for SPEEK, SCOF/SPEEK-75, and Nafion212 membranes, respectively. Reproduced with permission from Ref. [126]. Copyright 2025, Elsevier. (g) Schematic of iCOP-x membrane preparation. (h) Coulombic efficiency (CE) and (i) energy efficiency (EE) at various current densities of 60–180 mA cm^{-2}. Reproduced with permission from Ref. [127]. Copyright 2025, Elsevier.

actual flow battery operating conditions.

These tables reveal that recent advancements in membrane design, particularly those incorporating microporous architectures and tailored ion channels, have successfully pushed the boundaries of the traditional conductivity-selectivity trade-off.

4. Summary and perspectives

The development of advanced membranes for RFBs is critical to enabling grid-scale energy storage, yet it remains constrained by the fundamental conductivity–selectivity–stability trilemma. Traditional PFSA membranes offer high proton conductivity and durability but suffer from high cost, significant vanadium crossover, and environmental concerns. Hydrocarbon-based alternatives, while more affordable, often lack the chemical stability required for long-term operation in aggressive electrolytes. Here, this review first establishes the principles governing membrane performances, emphasizing ion transport mechanisms such as solution-diffusion in dense membranes and pore-

Table 3
Summary of membrane perporties.

Membrane	Thickness(μm)	Swelling radio(%)	Area resistance or ion conductivity	Test temperature(°C)	Vanadium permeability	Ref.
SPI-DH-60	60	15.39	101 mS cm^{-1}	80	1.38×10^{-7} cm^2 min^{-1}	[128]
1.5 %TPB-PBAP	55	14	74.5 mS cm^{-1}	180	4.6×10^{-8} cm^2 min^{-1}	[129]
MS-PBI #1	23	16	65 mS cm^{-1}	25	7.85×10^{-8} cm^2 min^{-1}	[87]
S52	52	34.6	39.2 mS cm^{-1}	Room temperature	6.85×10^{-14} cm^2 s^{-1}	[109]
s-OPBI 102	20	~35	29 mΩ cm^2 70 mS cm^{-1}	–	3.09×10^{-7} cm^2 min^{-1}	[130]
bipCTF/SP-100	69	~4	0.3 Ω cm^2	Room temperature	19.05×10^{-9} cm^2 s^{-1}	[131]
S/UiO-66-PS-2	59	~17	98.3 mS cm^{-1}	30	5.1×10^{-7} cm^2 s^{-1}	[132]
SPI-B-50	40	10	1.64×10^{-2} S cm^{-1} 0.24 Ω cm^2	–	0.71×10^{-7} cm^2 min^{-1}	[133]
b-DPM-N3	20–25	2.9	0.42 Ω cm^2	30	1.06×10^{-12} cm^2 s^{-1}	[134]

Table 4
Summary of membrane performances.

Membrane	Electrolyte	CE(%)	VE(%)	EE(%)	Cycle number	Current density (mA cm^{-2})	Ref.
C-abSPI-10	3 M SA	95–98.1	90.6–73.6	83.9	1500	120	[135]
SPI-DH-60	3 M SA	96.93	83.92	80.39	400	160	[128]
1.5 %TPB-PBAP	3 M SA	98.9	87.3	83.3	300	100	[129]
MS-PBI #1	3 M SA	99.6	~92	92.2	–	80	[87]
PSSP(1–25–25-1)	3 M SA	99.6	~83	88.5	3500	100	[109]
s-OPBI 102	3 M SA	98.6 ± 0.2	82.0 ± 1.1	91.8	200	80	[130]
HF-SCOF nano-pipeline ICM	3 M SA	99.5	82.3	81.9	1000	200	[136]
b-DPM-N3	0.5 M FcNCl/BTMAP-Vi	99	–	82–85	250	60	[134]

mediated flow in porous architectures. Key performance metrics, including conductivity, selectivity, and stability, are then deeply interlinked with material composition, water uptake, functional group density, and microstructural design.

Recent advancements in membrane design demonstrate innovative strategies across three primary architectures: dense, porous, and charged microporous membranes. Dense membranes, such as modified Nafion and sulfonated polyaromatics, leverage Donnan exclusion and hybrid approaches like supramolecular patching and bilayer designs to enhance selectivity without sacrificing conductivity. Porous membranes, fabricated via phase inversion or templating, utilize precise nanopore engineering for size-based ion sieving, significantly reducing area resistance while maintaining low crossover. Emerging charged microporous membranes combine rigid sub-nanometer channels with tailored surface chemistry to achieve simultaneous high conductivity and exceptional ion selectivity. These developments illustrate a shift toward multi-mechanistic and hierarchically structured membranes that decouple ion transport pathways from blocking mechanisms, offering promising routes to high-performance, durable, and sustainable RFBs.

Despite these advances, critical challenges persist. Long-term stability under harsh RFB conditions, such as extreme pH and oxidizing agents, remains elusive for non-fluorinated membranes. Scalable fabrication of membranes with sub-nanometer precision, which is essential for balancing high conductivity and selectivity, requires innovative processing techniques. Moreover, performance validation often relies on limited cycling data of <1000 cycles, insufficient for commercial RFBs demanding decade-long operation. And current assessment methods vary widely in terms of test cell configuration, electrolyte composition, current density, and cycling protocols, making it difficult to directly compare membrane performance across studies. The interdependence of membrane properties with redox couples and electrolytes further complicates universal design rules, necessitating system-specific optimization.

Based on the above summarized challenges, future efforts should prioritize four areas:

1) *Advanced modeling and characterization*: To rationally design next-generation membranes that overcome the conductivity–selectivity–stability trilemma, advanced computational and experimental tools are essential. Multiscale simulations spanning from molecular dynamics that elucidate atomistic interactions and ion transport mechanisms in sub-nanometer channels, to machine learning models that optimize microstructure and composition, must guide the design of membranes with tailored nanoarchitectures. Concurrently, operando characterization techniques, such as neutron scattering and X-ray imaging, should be employed to probe ion and water transport dynamics, swelling behavior, and degradation mechanisms in real time under realistic operating conditions. The integration of these approaches will provide fundamental insights into structure–property–performance relationships, accelerate the development of durable and high-performance membranes.

2) *Bio-inspired and multifunctional materials*: Next-generation membranes should leverage bio-inspired designs and multifunctional material strategies. This includes constructing hierarchical structures, such as artificial ion channels that mimic biological selectivity and efficiency, as well as gradient porosity for optimized ion transport and pressure distribution. Furthermore, integrating self-healing chemistries enabled by dynamic covalent bonds or supramolecular interactions could allow membranes to autonomously repair damage from mechanical stress or chemical degradation, thereby dynamically adapting to operational stresses, extending service life, and maintaining performance stability under fluctuating battery conditions.

3) *Standardized testing*: It's crucial to establish standardized testing protocols, particularly for evaluating long-term stability under harsh operational conditions. Developing unified benchmarks that simulate real-world stressors, such as extreme pH, highly oxidizing species, and prolonged operation, can accurately predict membrane durability over decades of service. Standardized validation will not only enable reliable screening of new materials but also accelerate the translation of laboratory innovations into commercially viable and durable membranes. This issue is compounded when comparing membranes tested in different RFB systems (e.g., VRFB vs. aqueous organic RFB).

4) *Integrated system design*: To bridge the lab-to-industry gap,

membrane development must extend beyond standalone material properties to holistic co-optimization with next-generation electrolytes, such as organic molecules and solid-phase suspensions under realistic flow conditions. This involves assessing long-term compatibility, crossover kinetics, and performance stability in operational environments to ensure scalability and system-level reliability for practical RFB applications. Furthermore, comprehensive techno-economic analysis and life cycle assessment (LCA) are becoming indispensable for justifying new membrane technologies. Evaluating the cost-per-cycle and overall environmental footprint, including resource use and end-of-life considerations, will provide critical metrics to validate the economic viability and sustainability of advanced membranes for grid-scale storage deployment.

CRediT authorship contribution statement

Jiaojiao Deng: Writing – review & editing, Writing – original draft, Validation, Methodology, Investigation, Formal analysis, Data curation. **Dongqing Pang:** Writing – review & editing, Methodology, Formal analysis, Data curation. **Xiaoliang Yu:** Writing – review & editing, Methodology, Formal analysis, Data curation. **Yu Bai:** Writing – review & editing, Methodology, Formal analysis, Data curation. **Jinhan Mo:** Writing – review & editing, Supervision, Project administration, Funding acquisition, Conceptualization.

Declaration of competing interest

The authors declare that they have no known competing financial interests or personal relationships that could have appeared to influence the work reported in this paper.

Acknowledgments

The authors gratefully acknowledge financial support from the National Natural Science Foundation of China (Nos. 52325801, 52402052).

Appendix A. Supplementary data

Supplementary data to this article can be found online at https://doi.org/10.1016/j.apenergy.2025.127316.

Data availability

No data was used for the research described in the article.

References

[1] Fell H, Gilbert A, Jenkins JD, Mildenberger M. Nuclear power and renewable energy are both associated with national decarbonization. Nat Energy 2022;7:25–9.
[2] Wu Y, Zhang T, Gao R, Wu C. Portfolio planning of renewable energy with energy storage technologies for different applications from electricity grid. Appl Energy 2021;287:116562.
[3] Li C, Hu L, Ren X, Lin L, Zhan C, Weng Q, et al. Asymmetric charge distribution of active centers in small molecule Quinone cathode boosts high-energy and high-rate aqueous zinc-organic batteries. Adv Funct Mater 2024;34:2313241.
[4] Ge B, Hu L, Yu X, Wang L, Fernandez C, Yang N, et al. Engineering triple-phase interfaces around the anode toward practical alkali metal–air batteries. Adv Mater 2024;36:2400937.
[5] Ge B, Deng J, Wang Z, Liang Q, Hu L, Ren X, et al. Aggregate-dominated dilute electrolytes with low-temperature-resistant ion-conducting channels for highly reversible Na plating/stripping. Adv Mater 2024;36:2408161.
[6] Deng J, Yu X, Tang J, Zhang L, Zhang K, Lin S, et al. Highly reversible lithium storage in a conversion-type $ZnCo_2O_4$ anode promoted by $NiCl_{2-x}F_x$ hydrate. J Mater Chem A 2020;8:2356–63.
[7] Zhao Y, Ma T, Hu L, Ren X, Sun X, Yu X. Supramolecular interaction chemistry in polymer electrolytes towards stable lithium metal batteries. J Energy Chem 2025;107:154–69.
[8] Guo Z, Sun J, Wan S, Wang Z, Ren J, Pan L, et al. Deep neural network-assisted fast and precise simulations of electrolyte flows in redox flow batteries. Appl Energy 2025;379:124910.
[9] Talebian R, Pourian A, Zakerabbasi P, Maghsoudy S, Habibzadeh S. Insights into energy efficiency for vanadium redox flow battery (VRFB) using the artificial intelligence technique. Appl Energy 2025;399:126485.
[10] Ye J, Xia L, Li H, de Arquer FPG, Wang H. The critical analysis of membranes toward sustainable and efficient vanadium redox flow batteries. Adv Mater 2024;36:2402090.
[11] Xiong P, Zhang L, Chen Y, Peng S, Yu G. A chemistry and microstructure perspective on ion-conducting membranes for redox flow batteries. Angew Chem Int Ed 2021;60:24770–98.
[12] Wang F, Ai F, Lu Y-C. Ion selective membrane for redox flow battery, what's next? Next Energy. 2023;1:100053.
[13] Safronova EY, Lysova AA, Voropaeva DY, Yaroslavtsev AB. Approaches to the modification of perfluorosulfonic acid membranes. Membranes 2023;13:721.
[14] Cremoncini D, Di Lorenzo G, Frate GF, Bischi A, Baccioli A, Ferrari L. Techno-economic analysis of aqueous organic redox flow batteries: stochastic investigation of capital cost and levelized cost of storage. Appl Energy 2024;360:122738.
[15] Lou X, Lu B, He M, Yu Y, Zhu X, Peng F, et al. Functionalized carbon black modified sulfonated polyether ether ketone membrane for highly stable vanadium redox flow battery. J Membr Sci 2022;643:120015.
[16] Upadhyay P, Sharma J, Mishra S, Mishra S, Kishore V, Kulshrestha V. Sulfanilic acid side-chain modified PEEK based membrane with dual functionality and proton selectivity for vanadium redox flow batteries. J Membr Sci 2025;717:123615.
[17] Zhang B, Zhao M, Liu Q, Zhang X, Fu Y, Zhang E, et al. Advanced anion exchange membranes with selective swelling-induced ion transport channels for vanadium flow battery application. J Membr Sci 2022;642:119985.
[18] Huang Z, Mu A, Wu L, Yang B, Qian Y, Wang J. Comprehensive analysis of critical issues in all-vanadium redox flow battery. ACS Sustain Chem Eng 2022;10:7786–810.
[19] Niccolai F, Guazzelli E, El Koura Z, Pucher I, Martinelli E. A critical update on the Design of Dense ion-Conducting Membranes for redox flow batteries. Adv Sustainable Syst 2025;9:2400661.
[20] Xu W, Long J, Liu J, Luo H, Duan H, Zhang Y, et al. A novel porous polyimide membrane with ultrahigh chemical stability for application in vanadium redox flow battery. Chem Eng J 2022;428:131203.
[21] Hua L, Lu W, Li T, Xu P, Zhang H, Li X. A highly selective porous composite membrane with bromine capturing ability for a bromine-based flow battery. Mater Today Energy 2021;21:100763.
[22] Sheng J, Li L, Wang H, Zhang L, Jiang S, Shi H. An ultrahigh conductivity and efficiency of SPEEK-based hybrid proton exchange membrane containing amphoteric GO-VIPS nanofillers for vanadium flow battery. J Membr Sci 2023;669:121326.
[23] Thangarasu S, Palanisamy G, Sadhasivam S, Selvakumar K, Neerugatti KRE, Oh TH. Deciphering the role of 2D graphene oxide nanofillers in polymer membranes for vanadium redox flow batteries. J Mater Chem A 2024;12:11176–234.
[24] Ye JY, Zheng CH, Liu J, Sun TF, Yu SH, Li HY. In situ grown tungsten trioxide nanoparticles on graphene oxide Nanosheet to regulate ion selectivity of membrane for high performance vanadium redox flow battery. Adv Funct Mater 2022;32:2109427.
[25] Pahlevaninezhad M, Miller EE, Yang L, Prophet LS, Singh A, Storwick T, et al. Exfoliated graphene composite membrane for the all-vanadium redox flow battery. ACS Appl Energy Mater 2023;6:6505–17.
[26] Lee J, Kim JQ, Ko H, Hwang I, Lee Y, Kim K, et al. Sub-20 nm ultrathin perfluorosulfonic acid-grafted graphene oxide composite membranes for vanadium redox flow batteries. J Membr Sci 2023;688:122150.
[27] Huynh TTK, Yang T, Nayanthara PS, Yang Y, Ye JY, Wang HX. Construction of high-performance membranes for vanadium redox flow batteries: challenges, development, and perspectives. Nano Micro Lett 2025;17:260.
[28] Kwabi DG, Ji YL, Aziz MJ. Electrolyte lifetime in aqueous organic redox flow batteries: a critical review. Chem Rev 2020;120:6467–89.
[29] Hollas A, Wei XL, Murugesan V, Nie ZM, Li B, Reed D, et al. A biomimetic high-capacity phenazine-based anolyte for aqueous organic redox flow batteries. Nat Energy 2018;3:508–14.
[30] Zhu QS, Ni LH, Peng K, Liu JX, Wu WB, Liang GF, et al. Fluorine-engineered membranes break the conductivity-selectivity trade-off in aqueous organic redox flow batteries. Angew Chem Int Ed 2025;64:e202510497.
[31] Zhang BG, Yang ZR, Liu Q, Liu YX, Jiang SN, Zhang XY, et al. High-performance aqueous organic redox flow battery enabled by sulfonated anthrone-containing poly(aryl ether ketone) membranes. J Membr Sci 2024;706:122968.
[32] Li CG, Han M, Xiang CM, Han R, Chen P. Double-layered anion exchange membrane for enhanced aqueous organic redox flow battery performance. ACS Appl Energy Mater 2025;8:9156–65.
[33] Mans N, Krieg HM, van der Westhuizen DJ. The effect of electrolyte composition on the performance of a single-cell Iron-chromium flow battery. Adv Energy Sust Res 2024;5:2300238.
[34] Wan CTC, Rodby KE, Perry ML, Chiang YM, Brushett FR. Hydrogen evolution mitigation in iron-chromium redox flow batteries via electrochemical purification of the electrolyte. J Power Sources 2023;554:232248.
[35] Waters SE, Robb BH, Marshak MP. Effect of chelation on Iron-chromium redox flow batteries. ACS Energy Lett 2020;5:1758–62.

[36] Cheng XS, Xuan T, Wang JC, Hu HR, Zhang DY, Zai JT, et al. Membrane contamination-driven sulfonate structuring for enhanced stability in all-iron redox flow batteries. Energy Storage Mater 2025;78:104226.
[37] Kreuer K-D, Münchinger A. Fast and selective ionic transport: from ion-conducting channels to ion exchange membranes for flow batteries. Annu Rev Mat Res 2021;51:21–46.
[38] Shehzad MA, Yasmin A, Ge X, Wu L, Xu T. A review of nanostructured ion-exchange membranes. Adv Mater Technol 2021;6:2001171.
[39] Kamcev J, Paul DR, Manning GS, Freeman BD. Predicting salt permeability coefficients in highly swollen, highly charged ion exchange membranes. ACS Appl Mater Interfaces 2017;9:4044–56.
[40] Sheng F, Wu B, Li X, Xu T, Shehzad MA, Wang X, et al. Efficient ion sieving in covalent organic framework membranes with sub-2-nanometer channels. Adv Mater 2021;33:2104404.
[41] Tan R, Wang A, Malpass-Evans R, Williams R, Zhao EW, Liu T, et al. Hydrophilic microporous membranes for selective ion separation and flow-battery energy storage. Nat Mater 2020;19:195–202.
[42] Tian E, Chen Q, Gao Y, Chen Z, Wang Y, Mo J. Advancing indoor air purification by mass transfer enhancement: bridging the gap between high-performance materials and technologies. Engineering 2025. https://doi.org/10.1016/j.eng.2025.07.003.
[43] Gao Y, Wang J, Tian E, Chen Z, Mo J. Electric-field activating on-surface tailored (OST) coarse polyester fibers for efficient airborne particle removal: interfacial morphologies and electrical response. Sep Purif Technol 2025;353:128291.
[44] Li X, Zuo P, Ge X, Yang Z, Xu T. Constructing new-generation ion exchange membranes under confinement regime. Natl Sci Rev 2025;12:nwae439.
[45] Wu Y, Jiang L, Wen L. Nanofluidic membrane for confined ion transport: from uniform to composite strategy. Mater Today 2023;65:189–206.
[46] Tsehaye MT, Mourouga G, Schmidt TJ, Schumacher JO, Velizarov S, Van der Bruggen B, et al. Towards optimized membranes for aqueous organic redox flow batteries: correlation between membrane properties and cell performance. Renew Sust Energy Rev 2023;173:113059.
[47] Ma J, Cai YC, Rong SD, Zhang MQ, Zhang JN, Han Z, et al. Dual-platform single-molecule redox-targeting reaction in neutral Anthraquinone flow batteries. ACS Nano 2025;19:27538–51.
[48] Jang JE, Kim RA, Jayasubramaniyan S, Lee CH, Choi J, Lee YD, et al. Full-Hexacyanometallate aqueous redox flow batteries exceeding 1.5 V in an aqueous solution. Adv Energy Mater. 2023;13:2300707.
[49] Dai Q, Zhao Z, Shi M, Deng C, Zhang H, Li X. Ion conductive membranes for flow batteries: design and ions transport mechanism. J Membr Sci 2021;632:119355.
[50] Tan R, Wang A, Ye C, Li J, Liu D, Darwich BP, et al. Thin film composite membranes with regulated crossover and water migration for long-life aqueous redox flow batteries. Adv Sci 2023;10:2206888.
[51] Wang JQ, Xu WY, Xu F, Dai LH, Wu YL, Wang YX, et al. A polybenzimidazole-covalent organic framework hybrid membrane with highly efficient proton-selective transport channels for vanadium redox flow battery. J Membr Sci 2024;695:122470.
[52] Sharma J, Gupta R, Ramanujam K, Kulshrestha V. Leveraging Long-life alkaline redox flow batteries using durable and high-hydroxide exchange N-bridged Triazine framework membranes. Small 2025;21:2406395.
[53] Pang D, Tian E, Xie R, Yin Z, Chen J, Deng J, et al. Advances and challenges in metal oxide semiconductor-based sensors for indoor ozone detection. Build Environ. 2025;285:113596.
[54] Wang A, Breakwell C, Foglia F, Tan R, Lovell L, Wei X, et al. Selective ion transport through hydrated micropores in polymer membranes. Nature 2024;635:353–8.
[55] Gao KW, Yu X, Darling RM, Newman J, Balsara NP. Increased Donnan exclusion in charged polymer networks at high salt concentrations. Soft Matter 2022;18:282–92.
[56] dos Santos FB, McMichael PS, Whitbeck A, Jalaee A, Gyenge E, Foster EJ. Proton exchange membranes from sulfonated lignin nanocomposites for redox flow battery applications. Small 2024;20:2309459.
[57] Myures XM, Suresh S, Arthanareeswaran G. Construction of thermal, chemical and mechanically stable ion exchange membranes with improved ion selectivity for vanadium redox flow batteries applications. J Power Sources 2024;591:233818.
[58] Kim S, Tighe TB, Schwenzer B, Yan J, Zhang J, Liu J, et al. Chemical and mechanical degradation of sulfonated poly (sulfone) membranes in vanadium redox flow batteries. J Appl Electrochem 2011;41:1201–13.
[59] Palanisamy G, Sadhasivam T, Park W-S, Bae ST, Roh S-H, Jung H-Y. Tuning the ion selectivity and chemical stability of a biocellulose membrane by PFSA ionomer reinforcement for vanadium redox flow battery applications. ACS Sustain Chem Eng 2020;8:2040–51.
[60] Xu K, Pei S, Zhang W, Han Z, Liu G, Xu X, et al. Chemical stability of proton exchange membranes synergistically promoted by organic antioxidant and inorganic radical scavengers. J Membr Sci 2022;655:120594.
[61] Wang FR, Luo S, Lei JF, Ai F, Leung KL, Fan J, et al. Nonfluorinated membrane with a decentralized ion-transport network enables efficient and sustainable polysulfide redox flow batteries. Sci Adv 2025;11:eaea0032.
[62] Xiong P, Li AM, Xiao SS, Jiang YQ, Peng SS, He Q. Supramolecular sidechain topology mediated Pseudo-nanophase separation engineering for high-performance redox flow battery membranes. Adv Energy Mater. 2024;14:2302809.
[63] Kim JQ, So S, Kim H-T, Choi SQ. Highly ordered ultrathin perfluorinated sulfonic acid ionomer membranes for vanadium redox flow battery. ACS Energy Lett 2020;6:184–92.
[64] Wang Q, Zhang ZJ, Lv PR, Peng Z, Yang JS. Poly(terphenyl pyridine) based amphoteric and anion exchange membranes with high ionic selectivity for vanadium redox flow batteries. Chem Eng J 2025;505:158922.
[65] Liang WQ, Ghasemiestahbanati E, Eden NT, Acharya D, Doherty CM, Majumder M, et al. Flow battery with remarkably stable performance at high current density: development of a nonfluorinated separator with concurrent rejection and conductivity. Angew Chem Int Ed 2025;64:e202505383.
[66] Liu HJ, Liu M, Zhang YT, Sun HZ, Ding CJ, Qian PH, et al. Ultrahigh ion selectivity composite membrane contained cationic covalent organic nanosheets for vanadium redox flow battery. J Membr Sci 2025;713:123314.
[67] Song W, Guo M, Tang YY, Wu JQ, Zhang ML, Su KM, et al. ZrO_2 nanofibers/sulfonated polysulfone-polysulfone composite membrane: achieving efficient alkaline water electrolysis through multivariable synergistic regulation. J Membr Sci 2025;735:124582.
[68] Golubenko DV, Van der Bruggen B, Yaroslavtsev AB. Novel anion exchange membrane with low ionic resistance based on chloromethylated/quaternized-grafted polystyrene for energy efficient electromembrane processes. J Appl Polym Sci 2020;137:48656.
[69] Hao X, Chen N, Chen Y, Chen D. Accelerated degradation of quaternary ammonium functionalized anion exchange membrane in catholyte of vanadium redox flow battery. Polym Degrad Stab 2022;197:109864.
[70] Su YK, Liu SQ, Shao B, Zhu WW, He Z, Wang J. Building water molecule chains in polybenzimidazole membrane toward superior vanadium redox flow battery. Chem Eng J 2024;485:149838.
[71] Duburg JC, Chen B, Holdcroft S, Schmidt TJ, Gubler L. Design of polybenzimidazolium membranes for use in vanadium redox flow batteries. J Mater Chem A 2024;12:6387–98.
[72] Wang Y, Feng K, Ding L, Wang L, Han X. Influence of solvent on ion conductivity of polybenzimidazole proton exchange membranes for vanadium redox flow batteries. Chin J Chem Eng 2020;28:1701–8.
[73] Duburg JC, Avaro J, Krupnik L, Silva BFB, Neels A, Schmidt TJ, et al. Design principles for high-performance Meta-Polybenzimidazole membranes for vanadium redox flow batteries. Energy Environ Mater 2025;8:e12793.
[74] Bui TT, Shin M, Rahimi M, Bentien A, Kwon Y, Henkensmeier D. Highly efficient vanadium redox flow batteries enabled by a trilayer polybenzimidazole membrane assembly. Carbon Energy 2024;6:e473.
[75] Ding L, Song X, Wang L, Zhao Z, He G. Preparation of dense polybenzimidazole proton exchange membranes with different basicity and flexibility for vanadium redox flow battery applications. Electrochim Acta 2018;292:10–9.
[76] Yan X, Dong Z, Di M, Hu L, Zhang C, Pan Y, et al. A highly proton-conductive and vanadium-rejected long-side-chain sulfonated polybenzimidazole membrane for redox flow battery. J Membr Sci 2020;596:117616.
[77] Bülbül E, Atanasov V, Mehlhorn M, Bürger M, Chromik A, Häring T, et al. Highly phosphonated polypentafluorostyrene blended with polybenzimidazole: application in vanadium redox flow battery. J Membr Sci 2019;570:194–203.
[78] Mishra S, Sharma J, Upadhyay P, Kulshrestha V. 2-Acrylamido-2-methylpropane sulfonic acid (AMPS) grafted poly (vinylidene fluoride)(PVDF) membrane for improved vanadium redox flow battery (VRFB) performance. Next Energy 2024;5:100164.
[79] Liu Z, Huang B, Li C, Zhu H, Liu G. Review of Progress in the application of polytetrafluoroethylene-based battery separators. ACS Appl Mater Interfaces 2024;16:63109–28.
[80] PS N, Sreenath S, Ash A, Pawar C, Dave V, Verma V, et al. Robust polyaniline-silica@ polypropylene for high-performance, high-capacity retention all-vanadium redox flow battery. ACS Appl Energy Mater 2024;7:2338–50.
[81] Qi HH, Pan LM, Sun J, Muzaffar N, Ren JY, Li HC, et al. Detecting and repairing micro defects in perfluorinated ion exchange membranes for redox flow batteries. J Power Sources 2025;628:235930.
[82] Zhang YX, Liu HJ, Liu M, Li XZ, Zhang YT, Sun HZ, et al. Enhanced selectivity of SPEEK membrane incorporated covalent organic nanosheet crosslinked graphene oxide for vanadium redox flow battery. J Membr Sci 2025;714:123410.
[83] Dai J, Dong Y, Yu C, Liu Y, Teng X. A novel Nafion-g-PSBMA membrane prepared by grafting zwitterionic SBMA onto Nafion via SI-ATRP for vanadium redox flow battery application. J Membr Sci 2018;554:324–30.
[84] Li Y, Sniekers J, Malaquias JC, Van Goethem C, Binnemans K, Fransaer J, et al. Crosslinked anion exchange membranes prepared from poly (phenylene oxide) (PPO) for non-aqueous redox flow batteries. J Power Sources 2018;378:338–44.
[85] Kusoglu A, Dursch TJ, Weber AZ. Nanostructure/swelling relationships of bulk and thin-film PFSA ionomers. Adv Funct Mater 2016;26:4961–75.
[86] Ikhsan MM, Abbas S, Do XH, Choi S-Y, Azizi K, Hjuler HA, et al. Polybenzimidazole membranes for vanadium redox flow batteries: effect of sulfuric acid doping conditions. Chem Eng J 2022;435:134902.
[87] Bui TT, Shin M, Abbas S, Ikhsan MM, Do XH, Dayan A, et al. Sulfonated para-Polybenzimidazole Membranes for Use in Vanadium Redox Flow Batteries15; 2025. p. 2401375.
[88] Pang B, Wu X, Yang M, Du R, Chen W, Yan X, et al. Anionic conductive group tunable amphoteric polybenzimidazole ion conductive membrane for vanadium redox flow battery. J Membr Sci 2023;670:121351.
[89] Yuan Z, Liang L, Dai Q, Li T, Song Q, Zhang H, et al. Low-cost hydrocarbon membrane enables commercial-scale flow batteries for long-duration energy storage. Joule 2022;6:884–905.
[90] Yang S, Chu X, Xue B, Lv T, Lin B, Zhang Z-H. Polyether ether ketone-based anion exchange membranes with bis-imidazolium cations for all-vanadium redox flow batteries. ACS Appl Energy Mater 2021;4:6787–96.

[91] Dai J, Wang K, Han X, Yan J, Teng X. Polysulfone-grafted poly (sodium styrene sulfonate)/polyvinylpyrrolidone amphoteric membranes for vanadium redox flow battery. Ionics 2024;30:889–99.
[92] Zhang Y, Zheng L, Liu B, Wang H, Shi H. Sulfonated polysulfone proton exchange membrane influenced by a varied sulfonation degree for vanadium redox flow battery. J Membr Sci 2019;584:173–80.
[93] Shi D, Li C, Yin Y, Lu W, Li G, Li X. Application of poly (ether sulfone)-based membranes in clean energy technology. Chem-Asian J 2023;18:e202201038.
[94] Zhao C, Xue J, Ran F, Sun S. Modification of polyethersulfone membranes–a review of methods. Prog Mater Sci 2013;58:76–150.
[95] Cornet N, Beaudoing G, Gebel G. Influence of the structure of sulfonated polyimide membranes on transport properties. Sep Purif Technol 2001;22:681–7.
[96] He Z, Wang G, Wei S, Li G, Zhang J, Chen J, et al. A novel fluorinated acid-base sulfonated polyimide membrane with sulfoalkyl side-chain for vanadium redox flow battery. Electrochim Acta 2021;399:139434.
[97] Do XH, Abbas S, Ikhsan MM, Choi SY, Ha HY, Azizi K, et al. Membrane assemblies with soft protective layers: dense and gel-type Polybenzimidazole membranes and their use in vanadium redox flow batteries. Small 2022;18:2206284.
[98] Kim JQ, Lee Y, Lee J, Rho Y, So S, Choi SQ. Engineered microdefects in Nano-membranes for enhanced ion selectivity and membrane durability in vanadium redox flow batteries. Small 2025;21:2206284.
[99] Wang AQ, Tan R, Liu DZ, Lu JX, Wei XC, Alvarez-Fernandez A, et al. Ion-selective microporous polymer membranes with hydrogen-bond and salt-bridge networks for aqueous organic redox flow batteries. Adv Mater 2023;35:2210098.
[100] Che X, Zhao H, Ren X, Zhang D, Wei H, Liu J, et al. Porous polybenzimidazole membranes with high ion selectivity for the vanadium redox flow battery. J Membr Sci 2020;611:118359.
[101] Peng K, Zhang C, Fang J, Cai H, Ling R, Ma Y, et al. Constructing microporous ion exchange membranes via simple Hypercrosslinking for pH-neutral aqueous organic redox flow batteries. Angew Chem Int Ed 2024;63:e202407372.
[102] Zuo P, Xu T. Constructing hydrophilic polymer membranes with microporosity for aqueous redox flow batteries. ChemSusChem 2025;18:e202402562.
[103] He GH, Li L, Xu H, Ji YL, Wang P. A polymer membrane with integrated microphase separation and intrinsic microporosity for aqueous organic redox flow batteries. Joule 2025;9:101976.
[104] Zhai L, Zhu Y-L, Wang G, He H, Wang F, Jiang F, et al. Ionic-nanophase hybridization of nafion by supramolecular patching for enhanced proton selectivity in redox flow batteries. Nano Lett 2023;23:3887–96.
[105] Zhai L, Chai S, Li T, Li H, He S, He H, et al. Self-assembled construction of ion-selective nanobarriers in electrolyte membranes for redox flow batteries. Nano Lett 2023;23:10414–22.
[106] Wang T, Cai Y, Ma J, Han Z, Rong S, Ye Q, et al. High-performance SPEEK membrane with polydopamine-bridged PTFE nanoparticles for vanadium redox flow batteries. J Energy Storage 2024;99:113318.
[107] Ye J, Zhao X, Ma Y, Su J, Xiang C, Zhao K, et al. Hybrid membranes dispersed with superhydrophilic TiO_2 nanotubes toward ultra-stable and high-performance vanadium redox flow batteries. Adv Energy Mater. 2020;10:1904041.
[108] Wang J, Xu W, Xu F, Dai L, Wu Y, Wang Y, et al. A polybenzimidazole-covalent organic framework hybrid membrane with highly efficient proton-selective transport channels for vanadium redox flow battery. J Membr Sci 2024;695:122470.
[109] Ikhsan MM, Abbas S, Do XH, Ha HY, Azizi K, Henkensmeier D. Sulfonated polystyrene/polybenzimidazole bilayer membranes for vanadium redox flow batteries. Adv Energy Mater. 2025;15:2400139.
[110] Xiong P, Peng S, Zhang L, Li A, Chen Y, Xiao S, et al. Supramolecular interactions enable pseudo-nanophase separation for constructing an ion-transport highway. Chem 2023;9:592–606.
[111] Xiong P, Li A, Xiao S, Jiang Y, Peng S, He Q. Supramolecular sidechain topology mediated Pseudo-nanophase separation engineering for high-performance redox flow battery membranes. Adv Energy Mater 2024;14:2302809.
[112] Sonne C, Jenssen BM, Rinklebe J, Lam SS, Hansen M, Bossi R, et al. EU need to protect its environment from toxic per-and polyfluoroalkyl substances. Sci Total Environ 2023;876:162770.
[113] Salmeron-Sanchez I, Bakvand PM, Shirole A, Avilés-Moreno JR, Ocón P, Jannasch P, et al. Zwitterionic poly (terphenylene piperidinium) membranes for vanadium redox flow batteries. Chem Eng J 2023;474:145879.
[114] Wan CTC, Jacquemond RR, Chiang YM, Nijmeijer K, Brushett FR, Forner-Cuenca A. Non-solvent induced phase separation enables designer redox flow battery electrodes. Adv Mater 2021;33:2006716.
[115] Dalal U, Kapoor M, Verma A. Low-cost pore-filled PVDF–Nafion composite membrane for the vanadium redox flow battery. Energ Fuel 2023;37:13457–66.
[116] Dai Q, Liu Z, Huang L, Wang C, Zhao Y, Fu Q, et al. Thin-film composite membrane breaking the trade-off between conductivity and selectivity for a flow battery. Nat Commun 2020;11:13.
[117] Li H, Zhu Q, Dong Y, Zuo P, Yang Z, Xu T. Ultra-microporous anion conductive membranes for crossover-free pH-neutral aqueous organic flow batteries. J Membr Sci 2023;668:121195.
[118] Shaheen I, Chiu W-H, Chen S-H, Lee K-M. MOF-& COF-integrated composite separators/membranes: innovations for sustainable and high-performance redox flow batteries. Sep Purif Technol 2025;376:134157.
[119] Xin L, Zhang D, Qu K, Lu Y, Wang Y, Huang K, et al. Zr-MOF-enabled controllable ion sieving and proton conductivity in flow battery membrane. Adv Funct Mater 2021;31:2104629.
[120] Cao H, Xia Y, Wang J, Ji H, Hong H, Xu K, et al. Shearing metal-organic framework lattice defects create low-resistance reservoir channels for high-performance aqueous organic flow battery. J Membr Sci 2025;717:123607.
[121] Zhang S, Wang G, Jing Y, Wei S, Wang B, Zhang Q, et al. A Novel Sulfonated Polyimide Composite Membrane Containing Covalent Organic Frameworks for Iron–Chromium Redox Flow Battery Application. Ind Eng Chem Res 2025;64:5995–6003.
[122] Sharma P, Shahi VK. Fabricating a partially fluorinated hybrid cation-exchange membrane for long durable performance of vanadium redox flow batteries. ACS Appl Mater Interfaces 2023;15:9171–81.
[123] Ye C, Wang A, Breakwell C, Tan R, Grazia Bezzu C, Hunter-Sellars E, et al. Development of efficient aqueous organic redox flow batteries using ion-sieving sulfonated polymer membranes. Nat Commun 2022;13:3184.
[124] Wang A, Tan R, Liu D, Lu J, Wei X, Alvarez-Fernandez A, et al. Ion-selective microporous polymer membranes with hydrogen-bond and salt-bridge networks for aqueous organic redox flow batteries. Adv Mater 2023;35:2210098.
[125] Wong T, Yang Y, Tan R, Wang A, Zhou Z, Yuan Z, et al. Sulfonated poly (ether-ether-ketone) membranes with intrinsic microporosity enable efficient redox flow batteries for energy storage. Joule 2025;9:101795.
[126] Ren Y, Wang S, Ma H, Yuan S, Zhao Q, Wadud MB, et al. Highly proton-conductive and stable sulfonated covalent organic framework hybrid membrane for vanadium redox flow battery. J Membr Sci 2025;722:123863.
[127] Wang Q, Song P, Zhang Y, Wang N, An Q-F. Ionic covalent organic polymer (iCOP) composite membranes with enhanced efficiency for iron-chromium redox flow battery. J Membr Sci 2025;722:123914.
[128] Jing YT, Wang G, Wei SG, Wang B, Zhang Q, Zhu WJ, et al. A novel sulfonated polyimide membranes inserting flexible decane chain and rigid triptycene-based crosslinked network for vanadium redox flow batteries. J Membr Sci 2025;734:124454.
[129] Shi N, Wang GR, Wang Q, Wang LL, Li QF, Yang JS. Acid doped branched poly (biphenyl pyridine) membranes for high temperature proton exchange membrane fuel cells and vanadium redox flow batteries. Chem Eng J 2024;489:151121.
[130] Bui TT, Park S, Shin M, Ikhsan MM, Kwon Y, Henkensmeier D. Sulfonated Polybenzimidazole membranes: how Sulfonation affects properties, stability, and performance in vanadium redox flow batteries. Adv Energy Mater. 2025;15:2500440.
[131] Qi MJ, Yan H, Wei W, Tang A. Covalent triazine frameworks crosslinked microporous polymer membranes with fast and selective ion transport for ultra-stable vanadium redox flow batteries. Chem Eng J 2024;497:155068.
[132] Zhang YX, Liu M, Liu HJ, Li XZ, Ding CJ, Zhang YT, et al. High ion-selective SPEEK-based composite membrane containing zwitterionic polymer-modified MOFs for vanadium redox flow battery. Chem Eng J 2025;516:164246.
[133] Li JC, Li HT, Duan HR, Long J, Huang WH, Yu YF, et al. Sulfonated polyimide membranes with branched architecture and unique diamine monomer for implementation in vanadium redox flow battery. J Power Sources 2024;591:233892.
[134] Yuan ZZ, Liang LX, Dai Q, Li TY, Song QL, Zhang HM, et al. Low-cost hydrocarbon membrane enables commercial-scale flow batteries for long-duration energy storage. Joule 2022;6:884–905.
[135] Zheng YX, Xu WY, Wu YL, Ding JY, Yu HW, You XZ, et al. A cross-linked sulfonated polyimide membrane with regulated acid-base interaction and high-performance for vanadium redox flow battery. J Membr Sci 2025;718:123651.
[136] Pang B, Xie GH, Zhao HM, Cui FJ, Liu CB, Chen WT, et al. SCOF hollow Fiber constructing ion selective conduction Nano-pipeline network for vanadium redox flow batteries. Adv Energy Mater. 2025;15:2500523.